TechBriefs

National Aeronautics and
Space Administration

Electronic Components and Circuits

Electronic Systems

Physical Sciences

Materials

Computer Programs

Mechanics

Machinery

Fabrication Technology

Mathematics and Information Sciences

Life Sciences

03-02 February 2003

INTRODUCTION

Tech Briefs are short announcements of innovations originating from research and development activities of the National Aeronautics and Space Administration. They emphasize information considered likely to be transferable across industrial, regional, or disciplinary lines and are issued to encourage commercial application.

Availability of NASA Tech Briefs and TSPs

Requests for individual Tech Briefs or for Technical Support Packages (TSPs) announced herein should be addressed to

National Technology Transfer Center
Telephone No. **(800) 678-6882** or via World Wide Web at **www2.nttc.edu/leads/**

Please reference the control numbers appearing at the end of each Tech Brief. Information on NASA's Commercial Technology Team, its documents, and services is also available at the same facility or on the World Wide Web at **www.nctn.hq.nasa.gov**.

Commercial Technology Offices and Patent Counsels are located at NASA field centers to provide technology-transfer access to industrial users. Inquiries can be made by contacting NASA field centers and program offices listed below.

NASA Field Centers and Program Offices

Ames Research Center
Carolina Blake
(650) 604-1754 or
cblake@mail.arc.nasa.gov

Dryden Flight Research Center
Jenny Baer-Riedhart
(661) 276-3689 or
jenny.baer-riedhart@dfrc.nasa.gov

Goddard Space Flight Center
George Alcorn
(301) 286-5810 or
galcorn@gsfc.nasa.gov

Jet Propulsion Laboratory
Merle McKenzie
(818) 354-2577 or
merle.mckenzie@jpl.nasa.gov

Johnson Space Center
Charlene E. Gilbert
(281) 483-3809 or
commercialization@jsc.nasa.gov

John F. Kennedy Space Center
Jim Aliberti
(321) 867-6224 or
Jim.Aliberti-1@ksc.nasa.gov

Langley Research Center
Sam Morello
(757) 864-6005 or
s.a.morello@larc.nasa.gov

Glenn Research Center
Larry Viterna
(216) 433-3484 or
cto@grc.nasa.gov

George C. Marshall Space Flight Center
Vernotto C. McMillan
(256) 544-2615 or
vernotto.mcmillan@msfc.nasa.gov

John C. Stennis Space Center
Kirk Sharp
(228) 688-1929 or
technology@ssc.nasa.gov

NASA Program Offices
At NASA Headquarters there are seven major program offices that develop and oversee technology projects of potential interest to industry:

Carl Ray
Small Business Innovation Research Program (SBIR) & Small Business Technology Transfer Program (STTR)
(202) 358-4652 or
cray@mail.hq.nasa.gov

Dr. Robert Norwood
Office of Commercial Technology (Code RW)
(202) 358-2320 or
rnorwood@mail.hq.nasa.gov

John Mankins
Office of Space Flight (Code MP)
(202) 358-4659 or
jmankins@mail.hq.nasa.gov

Terry Hertz
Office of Aero-Space Technology (Code RS)
(202) 358-4636 or
thertz@mail.hq.nasa.gov

Glen Mucklow
Office of Space Sciences (Code SM)
(202) 358-2235 or
gmucklow@mail.hq.nasa.gov

Roger Crouch
Office of Microgravity Science Applications (Code U)
(202) 358-0689 or
rcrouch@hq.nasa.gov

Granville Paules
Office of Mission to Planet Earth (Code Y)
(202) 358-0706 or
gpaules@mtpe.hq.nasa.gov

TechBriefs

National Aeronautics and
Space Administration

February 2003
03-02

Electronic Components and Circuits

Hardware, Techniques, and Processes

Integrated Electrode Arrays for Neuro-Prosthetic Implants

Integrated array would eliminate the need for extensive cabling in implants.

NASA's Jet Propulsion Laboratory, Pasadena, California

Arrays of electrodes integrated with chip-scale packages and silicon-based integrated circuits have been proposed for use as medical electronic implants, including neuro-prosthetic devices that might be implanted in brains of patients who suffer from strokes, spinal-cord injuries, or amyotrophic lateral sclerosis. The electrodes of such a device would pick up signals from neurons in the cerebral cortex, and the integrated circuit would perform acquisition and preprocessing of signal data. The output of the integrated circuit could be used to generate, for example, commands for a robotic arm.

Electrode arrays capable of acquiring electrical signals from neurons already exist, but heretofore, there has been no convenient means to integrate these arrays with integrated-circuit chips. Such integration is needed in order to eliminate the need for the extensive cabling now used to pass neural signals to data-acquisition and -processing equipment outside the body. The proposed integration would enable progress toward neuro-prostheses that would be less restrictive of patients' mobility.

An array of electrodes would comprise a set of thin wires of suitable length and composition protruding from and supported by a fine-pitch micro-ball grid array or chip-scale package (see figure). The associated integrated circuit would be mounted on the package face opposite the probe face, using the solder bumps (the balls of the ball grid array) to make the electrical connections between the probes and the input terminals of the integrated circuit. The key innovation is the insertion of probe wires of the appropriate length and material into the solder bumps through a reflow process, thereby fixing the probes in place and electrically connecting them with the integrated circuit.

The probes could be tailored to any distribution of lengths and made of any suitable metal that could be drawn into fine wires. Furthermore, the wires could be coated with an insulating layer using anodization or other processes, to achieve the correct electrical impedance. The probe wires and the packaging materials must be biocompatible using such materials as lead-free solders. For protection, the chip and package can be coated with parylene.

This work was done by Erik Brandon and Mohammed Mojarradi of Caltech for **NASA's Jet Propulsion Laboratory**. *For further information, access the Technical Support Package (TSP)* ***free on-line at www.nasatech.com*** *under the category.*

In accordance with Public Law 96-517, the contractor has elected to retain title to this invention. Inquiries concerning rights for its commercial use should be addressed to

Intellectual Property group
JPL
Mail Stop 202-233
4800 Oak Grove Drive
Pasadena, CA 91109
(818) 354-2240

Refer to NPO-21198, volume and number of this NASA Tech Briefs *issue, and the page number.*

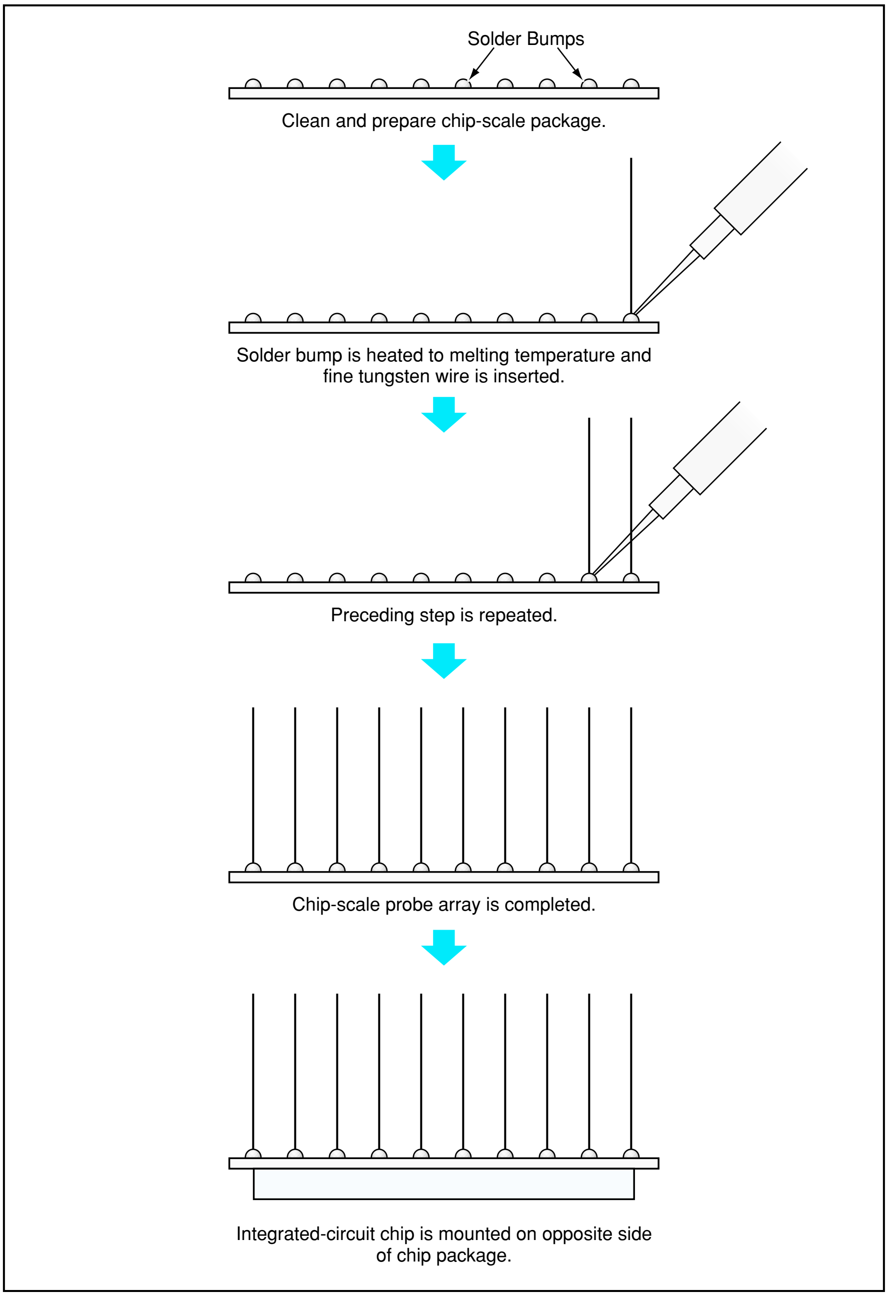

Conceptual Process Flow shows wires supported and electrically connected by solder bumps, which would serve as electrodes for acquiring signals from neurons. The integrated circuit would preprocess the signals for use by external circuits.

Eroding Potentiometers

These simple transducers can be used to measure advances of char fronts.

Marshall Space Flight Center, Alabama

Eroding potentiometers have been devised for measuring the time-dependent positions of char fronts advancing through layers of insulating material subject to intense heating from one side. In the original application, the material layers of interest are thermal insulators in rocket motors and the heat comes from firing of the motors, but the principle of operation is equally applicable to other insulating materials subject to intense heating (e.g., ablative fire-retardant materials). Measuring the thickness decrement of propellant (in hybrid motors in particular) is another possible application of this transducer. Telemetry informs mission control of the propellant left after each burn.

An eroding potentiometer could be characterized, more precisely, as an eroding two-wire resistor. It includes a twisted pair of thin, insulated wires oriented along the thickness of, and embedded in, the layer of thermal-insulation material to be tested (see figure). The electrical insulation material on the wires should be one for which the charring temperature is about the same as (or perhaps slightly less than) that of the thermal-insulation material to be tested. In the original rocket-motor application, the wires have a diameter of 0.003 in. (≈0.08 mm), are made of manganin, and are coated with polyimide for electrical insulation. Outside the thermal insulation on the cold side, the wire leads are connected to a Wheatstone bridge circuit for measurement of electrical resistance change.

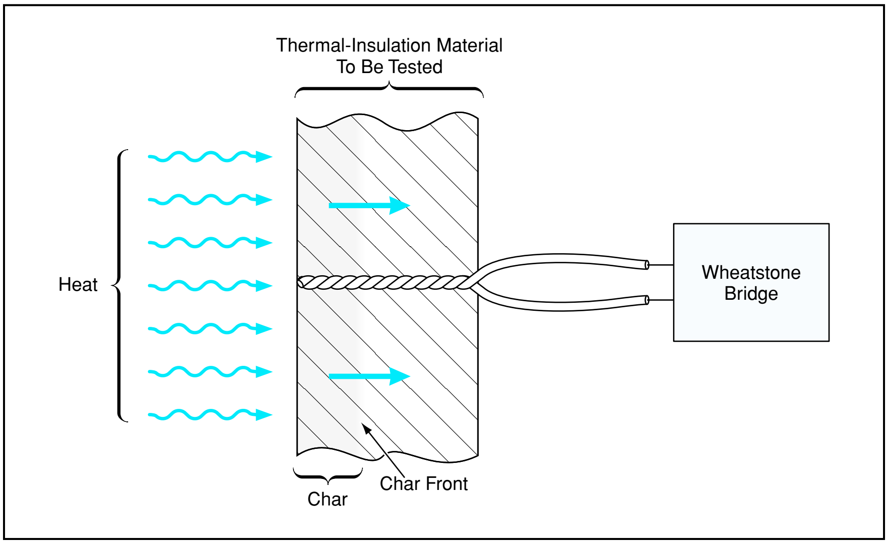

A **Twisted Pair of Electrically Insulated Wires** can be used to measure the advance of the char front in real time: The intermittent short-circuit resistance of the twisted pair, as measured by the Wheatstone bridge, varies with position of the char front.

Before the formation of the char front, there is an open circuit between the wires, so that the resistance sensed by the Wheatstone bridge is very high. As the char front advances along the twisted pair of wires, the char intermittently forms short circuits between the wires. Optionally, one could add a third, bare wire (possibly made of aluminum) to the twisted pair to increase the likelihood of forming low-resistance short circuits. The intervals between occurrences of short circuits can be considered short in the sense that, during each interval, the char front advances only a small fraction of the thickness of the thermal-insulation material under test.

During each short-circuit interval, the resistance sensed by the Wheatstone bridge is approximately linearly related to the length of remaining wire that has not yet been reached by the char front. Putting it somewhat differently, the decrease in resistance from one short-circuit reading to the next is approximately proportional to the distance traveled by the char front between the readings. Thus, once one has performed a calibration to establish the relationship between the short-circuit resistance reading and the position of the char front, one can, thereafter, infer the instantaneous position of the char front from the most recent short-circuit resistance readings.

In the original rocket-motor application, a decrease in resistance of ≈3 Ω corresponds to a char-front advance of ≈0.5 in. (≈1.3 cm). In practice, when one uses a typical Wheatstone bridge to measure the resistance in such an application, the output potential of the bridge switches intermittently between a short-circuit value of a few millivolts and an open-circuit value of ≈2.5 V. One must process the output potential through an amplifier capable of fast recovery to the proper setting point after saturation in order to be able to correctly amplify the small short-circuit potential each time a short circuit occurs and the wire resistance up to the char front is sensed briefly.

This work was done by Mark Eggett, John L. Shipley, Alan L. Godfrey, Lloyd T. Johnson, Mont Johnson, Boyd D. Bryner, and Bruce McWhorter of Thiokol Corp. for **Marshall Space Flight Center**. *For further information, please contact George Alford at Thiokol Propulsion at (435) 863-3954.*
MFS-31437

Common/Dependent-Pressure-Vessel Nickel-Hydrogen Batteries

One of the principal advantages would be high volumetric efficiency.

NASA's Jet Propulsion Laboratory, Pasadena, California

The term "common/dependent pressure vessel" (C/DPV) denotes a proposed alternative configuration for a nickel-hydrogen battery. The C/DPV configuration is so named because it is a hybrid of two prior configurations called "common pressure vessel" (CPV) and "dependent pressure vessel" (DPV). The C/DPV configuration has been proposed as a basis for designing highly reliable, long-life Ni/H_2-batteries and cells for anticipated special applications in which it is expected that small charge capacities will suffice and sizes and weights must be minimized.

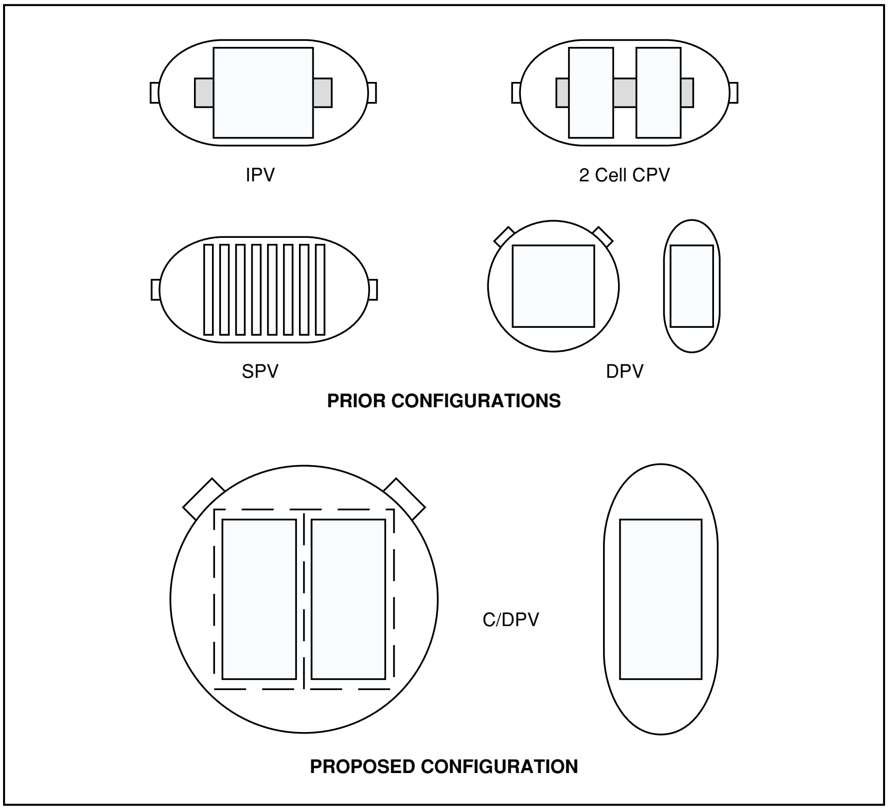

The **C/DPV Configuration** would be a hybrid of the older CPV and DPV configurations (and, to some extent, of the SPV configuration). Modular designs could provide ranges of capacities and voltages.

The figure depicts examples of the proposed C/DPV configuration along with the CPV and DPV configurations and two other prior configurations called "individual pressure vessel" (IPV) and "single pressure vessel" (SPV). The following characteristics of the prior configurations are particularly relevant to the proposal of the C/DPV configuration:

- A DPV has a pocket-watch shape that is both advantageous and disadvantageous, in comparison with the shapes of the IPV, CPV, and SPV. The advantage is that a battery or cell can be made relatively flat and thin to fit in a thin space; the disadvantage is that a pressure vessel of this shape is not self-supporting and therefore must be mounted between objects that restrain it. DPV cells have not been widely used.
- The SPV and CPV configurations have been the basis of the established method for designing pressure vessels containing multiple cells.

Like the CPV and SPV configurations, the C/DPV configuration is one of multiple cells contained within a DPV. This configuration would afford the advantages and disadvantages of the DPV configuration (thinness and the need for mechanical restraint, respectively), while making it possible to use an electrolyte-containment system like that of the SPV. Although it is not readily apparent by visual examination of the figure, calculations have shown that for a given small charge capacity, the volumetric efficiency of a battery in the C/DPV configuration would exceed the volumetric efficiencies of batteries in the other configurations mentioned. Other anticipated advantages of the C/DPV configuration include improved thermal properties, greater simplicity and reliability (in comparison with the SPV configuration), lower costs associated with the simpler designs, and amenability to replacement and matching of cells.

This work was done by Paul J. Timmerman of Caltech for **NASA's Jet Propulsion Laboratory**. *Further information is contained in a TSP [see page 1].*
NPO-20769

120-GHz HEMT Oscillator With Surface-Wave-Assisted Antenna

This is a compact, lightweight alternative to vacuum-tube oscillators.

NASA's Jet Propulsion Laboratory, Pasadena, California

Two monolithic microwave integrated circuits (MMICs) have been designed and built to function together as a source of electromagnetic radiation at a frequency of 120 GHz. One of the MMICs is an oscillator and is the highest-power 120-GHz oscillator reported thus far in the literature. The other MMIC is an end-fire antenna that radiates the oscillator signal. Although these MMICs were constructed as separate units and electrically connected with wire bonds, future oscillator/antenna combinations could readily be fabricated as monolithic integrated units. Such units could be used as relatively high-power solid-state microwave sources in diverse applications that include automotive radar, imaging, scientific instrumentation, communications, and radio astronomy. As such, these units would be attractive alternatives to vacuum-tube oscillators, which are still used to obtain acceptably high power in the frequency range of interest.

The oscillator (see figure) includes a high-electron-mobility transistor (HEMT), with gate-periphery dimensions of 4 by 37 μm, in a common-source configuration. The series feedback element of the oscillator is a grounded coplanar waveguide (CPW) at the source. The HEMT is biased for class-A operation (meaning that current is conducted throughout the oscillation cycle) to maximize the output power of the oscillator. Input and output impedance-matching circuit elements are designed to maximize output power and to establish the conditions needed for oscillation.

The design of the antenna takes advantage of surface waves, which, heretofore, have been regarded as highly disadvantageous because they can leak power and degrade the performances of antennas that have not been designed to exploit them. Measures taken to suppress surface waves have included complex machining of circuit substrates and addition of separate substrates. These measures are difficult to implement in standard MMIC fabrication processes. In contrast, because the design of the present antenna eliminates the need to suppress surface waves, the fabrication of the antenna is fully compatible with standard MMIC fabrication processes.

The design of this antenna is a specific instance of a quasi-Yagi generic antenna design (so named because of a resemblance to the classic Yagi-Uda dipole-array antenna design). The design relies on the generation of the TE_0 surface wave as its primary source of free-space radiation. For this reason, the antenna is best suited for fabrication on a substrate that has a high permittivity, making it ideal for integration into an MMIC that is fabricated on an InP or GaAs substrate. Contrary to convention in the design of printed dipole antennas, the grounded metal of the feed line of the antenna is used as a surface-wave-reflecting element that helps to form the radiation into a unidirectional, end-fire beam. The antenna radiates efficiently over a broad frequency band; it is also suitable for use as a transition from the planar MMIC to a waveguide.

In a test, the oscillator-and-antenna combination was found to radiate power along the antenna's end-fire direction into a WR8 open-ended waveguide and power meter. After correction for the gain of the receiving antenna and the free-space loss, the effective isotropically radiated power (EIRP) was estimated to be 12 dBm. The isotropic conversion gain (defined as the ratio between the EIRP and the DC input power) at the frequency of 120 GHz was found to be 18 percent.

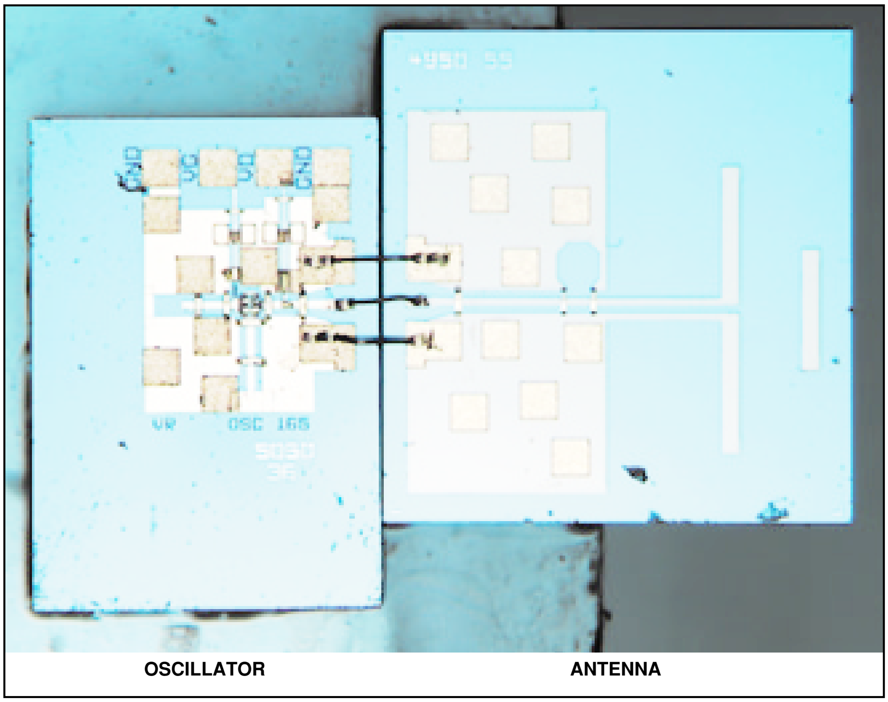

This **Oscillator and Antenna** are MMIC components of a prototype compact, lightweight, relatively high-power, 120-GHz source. Future versions could readily be fabricated as single, monolithic MMICs.

This work was done by Lorene Samoska and Peter Siegel of **NASA's Jet Propulsion Laboratory***; Kevin Leong, Tatsuo Itoh, and Yongxi Qian of UCLA; and Vesna Radisic of HRL Laboratories, LLC. Further information is contained in a TSP [see page 1].*
NPO-21246

80-GHz MMIC HEMT Voltage-Controlled Oscillator

Output power and tuning range exceed those of prior HEMT-based oscillators.

NASA's Jet Propulsion Laboratory, Pasadena, California

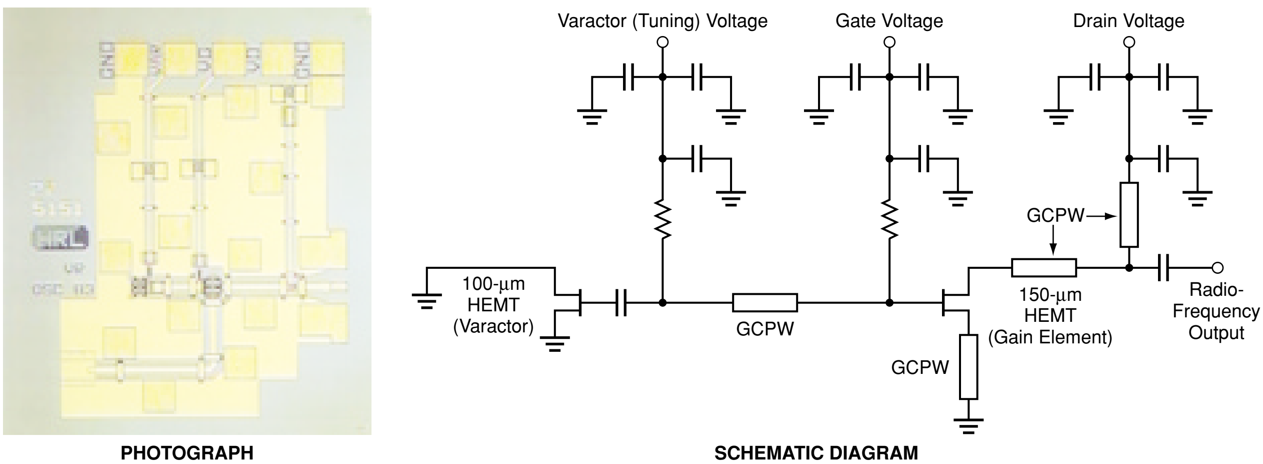

Figure 1. This **MMIC HEMT Oscillator** occupies a chip with dimensions of 1.22 mm by 1.3 mm by 50 µm.

A voltage-controlled oscillator (VCO) that operates in the frequency range from 77.5 to 83.5 GHz has been constructed in the form of a monolithic microwave integrated circuit (MMIC) that includes high-electron-mobility transistors (HEMTs). This circuit is a prototype of electronically tunable signal sources in the 75-to-110-GHz range, needed for communication, imaging, and auto-

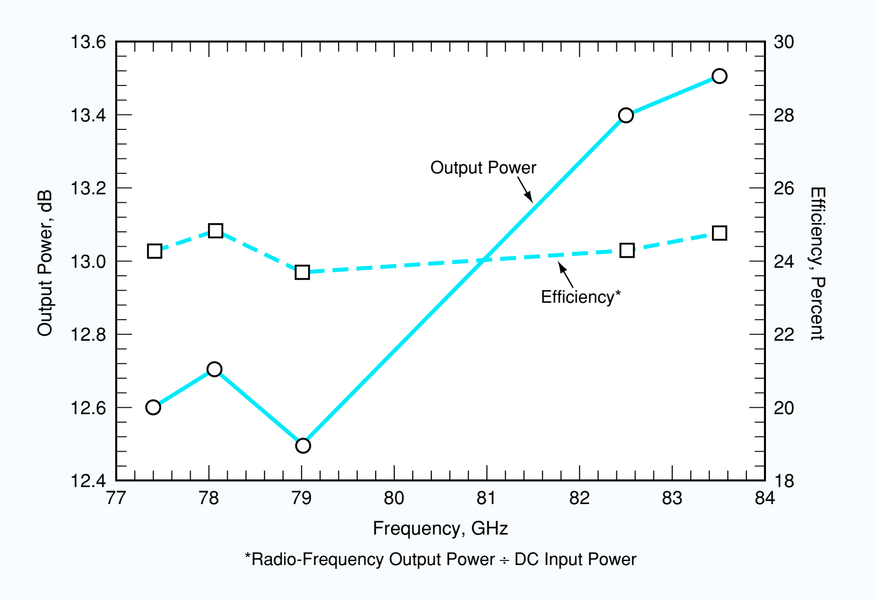

Figure 2. The **Output Power and Power Efficiency** of the frequency oscillator were measured as functions of frequency over its 6-GHz-wide tuning range.

motive radar applications, among others.

This oscillator (see Figure 1) includes two AlInAs/GaInAs/InP HEMTs. One HEMT serves mainly as an oscillator gain element. The other HEMT serves mainly as a varactor for controlling the frequency: the frequency-control element is its gate-to-source capacitance, which is varied by changing its gate supply voltage.

The gain HEMT is biased for class-A operation (meaning that current is conducted throughout the oscillation cycle). Grounded coplanar waveguides are used as impedance-matching transmission lines, the input and output matching being chosen to sustain oscillation and maximize output power. Air bridges are placed at discontinuities to suppress undesired slot electromagnetic modes. A high density of vias is necessary for suppressing a parallel-plate electromagnetic mode that is undesired because it can propagate energy into the MMIC substrate.

Previous attempts at constructing HEMT-based oscillators yielded circuits with relatively low levels of output power and narrow tuning ranges. For example, one HEMT VCO reported in the literature had an output power of 7 dBm (≈5 mW) and a tuning range 2-GHz wide centered approximately at a nominal frequency of 77 GHz. In contrast, as shown in Figure 2, the present MMIC HEMT VCO puts out a power of 12.5 dBm (≈18 mW) or more over the 6-GHz-wide frequency range from 77.5 to 83.5 GHz.

This work was done by Lorene Samoska of ***NASA's Jet Propulsion Laboratory*** *and Vesna Radisic, Miro Micovic, Ming Hu, Paul Janke, Catherine Ngo, and Loi Nguyen of HRL Laboratories, LLC. Further information is contained in a TSP [see page 1].*
NPO-21214

High-Energy-Density Capacitors

Maximum sustainable energy density is more than twice that of polypropylene-film capacitors.

John H. Glenn Research Center, Cleveland, Ohio

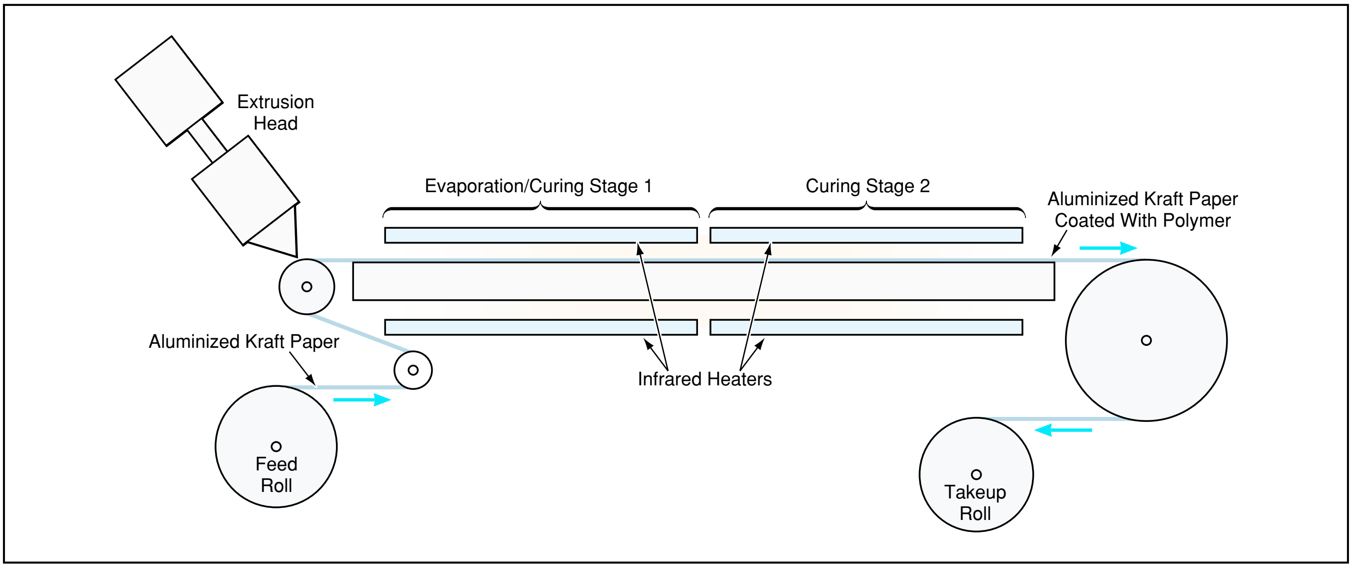

A **Film of Dielectric Polymer Is Cast** on a continuous strip of aluminized kraft paper. High dielectric performance is obtained through selection of the materials and design of the process and machinery.

Capacitors capable of storing energy at high densities are being developed for use in pulse-power circuits in such diverse systems as defibrillators, particle-beam accelerators, microwave sources, and weapons. Like typical previously developed energy-storage capacitors, these capacitors are made from pairs of metal/solid-dielectric laminated sheets that are wound and pressed into compact shapes to fit into cans, which are then filled with dielectric fluids. Indeed, these capacitors can be fabricated largely by conventional fabrication techniques. The main features that distinguish these capacitors from previously developed ones are improvements in (1) the selection of laminate materials, (2) the fabrication of the laminated sheets from these materials, and (3) the selection of dielectric fluids.

In simplest terms, a high-performance laminated sheet of the type used in these capacitors is made by casting a dielectric polymer onto a sheet of aluminized kraft paper. The dielectric polymer is a siloxane polymer that has been modified with polar pendant groups to increase its permittivity and dielectric strength.

Potentially, this polymer is capable of withstanding an energy density of 7.5 J/cm^3, which is four times that of the previous state-of-the-art-capacitor dielectric film material. However, the full potential of this polymer cannot be realized at present because (1) at thicknesses needed for optimum performance (≤8.0 μm), the mechanical strength of a film of this polymer is insufficient for incorporation into a wound capacitor and (2) at greater thickness, the achievable energy density decreases because of a logarithmic decrease in dielectric strength with increasing thickness. The aluminized kraft paper provides the mechanical strength needed for processing of the laminate and fabrication of the capacitor, and the aluminum film serves as an electrode layer. Because part of the thickness of the dielectric is not occupied by the modified siloxane polymer, the achievable energy density must be somewhat less than the maximum value.

The laminate is produced by a continuous film-casting process, using the machinery depicted schematically in the figure. The designs of the process and machinery are dictated partly by the fact that during the processing step prior to casting the polymer, the aluminized kraft paper becomes wet with water. Because the polymer resin to be cast is hydrophobic, the paper must be dried to make it possible to coat the paper uniformly, leaving no pinholes. Accordingly, an infrared heater is placed next to the paper feed roll to dry the paper prior to casting.

The polymer is cast onto the aluminized paper by an extrusion head. To ensure uniform thickness of the cast film, the designs of the extrusion head and the apparatus that feeds the resin to the head incorporate several refinements. To prevent undesired increases in viscosity, blockages, and other undesired effects of premature polymerization, the resin and the extrusion head are cooled to 0 °C to retard polymerization until the moment of casting. Downstream of the extrusion head, the resin-coated aluminized paper is heated to cure the polymer.

A total of ten dielectric fluids were evaluated with regard to their properties, compatibility with the polymer-coated kraft paper, and effect on the dielectric strength of the polymer. This evaluation led to the selection of castor oil as the dielectric fluid (with mineral oil and fluorinated siloxane as alternates for situations in which the use of castor oil would be problematic).

Experimental capacitors made from windings of the polymer-coated aluminized kraft paper with castor-oil and mineral-oil impregnation exhibited state-of-the-art performance. Notable among the performance characteristics was the ability to withstand energy densities up to 2.5 J/cm^3; although this is less than the theoretical maximum, it is more than double the maximum energy density of polypropylene-film capacitors now in use.

This work was done by Kirk Slenes of TPL, Inc., for **Glenn Research Center**. *Further information is contained in a TSP [see page 1].*

Inquiries concerning rights for the commercial use of this invention should be addressed to NASA Glenn Research Center, Commercial Technology Office, Attn: Steve Fedor, Mail Stop 4–8, 21000 Brookpark Road, Cleveland, Ohio 44135. Refer to LEW-16921.

Physical Sciences

Hardware, Techniques, and Processes

Books and Reports

Microscale Thermal-Transpiration Gas Pump

This is a prototype of miniature vacuum pumps with no moving parts.

NASA's Jet Propulsion Laboratory, Pasadena, California

A recent addition to the growing class of microelectromechanical systems (MEMS) is a single stage of a Knudsen compressor. This device was fabricated and tested to demonstrate the feasibility of Knudsen compressors as miniature vacuum pumps for future portable scientific instruments. The attributes of Knudsen compressors that make them attractive as miniature vacuum pumps are that they contain no moving parts and operate without need for lubricants or working fluids.

A Knudsen compressor exploits thermal transpiration of a rarefied gas. The principle of thermal transpiration can be described in terms of an example of two volumes of gas at different temperatures T_1 and T_2 connected by a tube with a radius smaller than the mean free path (λ) of gas molecules. The behavior of this system depends on the Knudsen number ($Kn \equiv \lambda/L$, where L is a characteristic linear dimension of the tube): For Kn less than about 0.01 λ/L, the gas flows as a continuum; for Kn between about 0.01 and 10, the flow behavior of the gas is transitional between the continuum and free-molecular regimes; for Kn of about 10 or more, the flow regime is free-molecular. In the free-molecular regime, simple balancing of the equilibrium molecular fluxes leads to the following equation for the equilibrium pressures in the two volumes:

$$p_1/p_2 = (T_1/T_2)^{1/2}.$$

The pressure differential can be exploited for pumping.

The advent of MEMS fabrication techniques and of nanopore materials with low thermal conductivities has made it possible to exploit thermal transpiration as more than a laboratory curiosity. This is because passages in pumping devices can now be made so narrow that transitional or free-molecular flow conditions can be obtained in these devices, even at pressures as high as atmospheric.

A Knudsen compressor is a cascade of multiple, individually heated compressor stages that exploit thermal transpiration. Figure 1 is a simplified schematic diagram of single stage, which includes a capillary and a connector section. By virtue of thermal transpiration, an increase in temperature along the capillaries results in an increase in pressure along the capillaries. The capillary section is followed by the connector section, where the pressure is approximately constant while the temperature falls to its lower value prior to entry to the next stage. The difference in pressure between the hotter and colder sides depends on the Kn values and other parameters; in general, it increases with the transition from the continuum to the free-molecular regime.

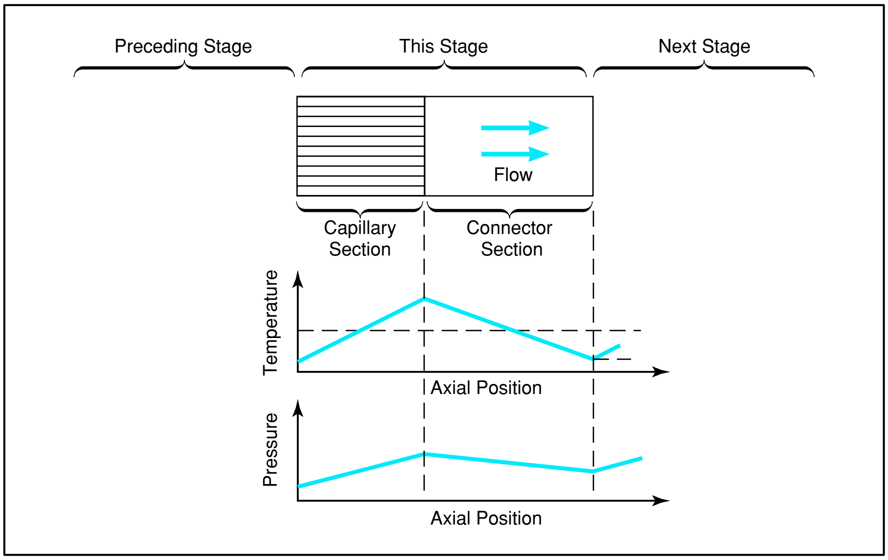

Figure 1. **One Stage of a Knudsen Compressor** exploits thermal transpiration to sustain a small net increase in pressure. Multiple stages like this one are cascaded in order to sustain a usefully large overall increase in pressure.

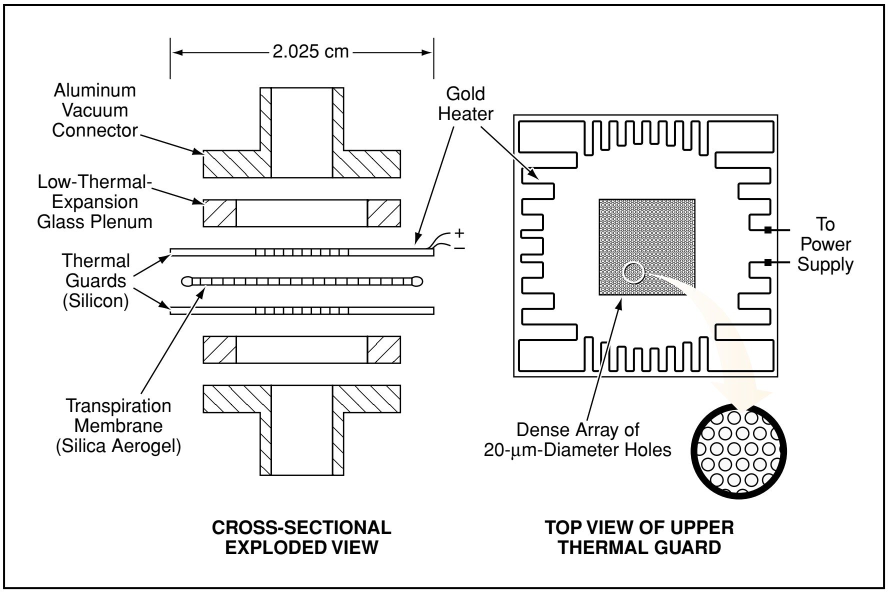

Figure 2. **Advanced Materials and Fabrication Techniques** are essential to the realization of this prototype of a one stage of a microscale Knudsen compressor. The transpiration medium is a 520-µm-thick SiO_2-aerogel membrane. The hot- and cold-side thermal guards are 400-µm-thick micromachined silicon chips.

The prototype microscale single Knudsen compressor stage (see Figure 2) includes two silicon chips that serve as hot-side and cold-side thermal guards (the hot-side thermal guard corresponding approximately to the connector section described above), an SiO_2-aerogel membrane (corresponding approximately to the capillary section described above), two low-thermal-expansion glass plenums, and aluminum vacuum connectors. The role of the thermal guards is to adjust the temperatures of molecules to the desired different values on the opposite sides of the aerogel transpiration membrane: Each silicon chip contains a dense array of 20-μm-diameter through holes, made by deep reactive-ion etching, that serve as tubes for heating or cooling the gas in them. Thin gold film heaters are patterned on both silicon chips; hence, either silicon chip can be the hot-side thermal guard. The aerogel has an average pore size of 20 nm and a very low thermal conductivity (17 W/K at atmospheric pressure), and thus satisfies the essential requirements for thermal transpiration to occur when a voltage is applied to one of the heaters.

This work was done by Stephen Vargo, E. Phillip Muntz, and Geoff Shiflett of Caltech for **NASA's Jet Propulsion Laboratory**. *Further information is contained in a TSP [see page 1].*
NPO-21110

Instrument for Measuring Temperature of Water

An infrared radiometer is able to view water as an almost pure blackbody source.

Stennis Space Center, Mississippi

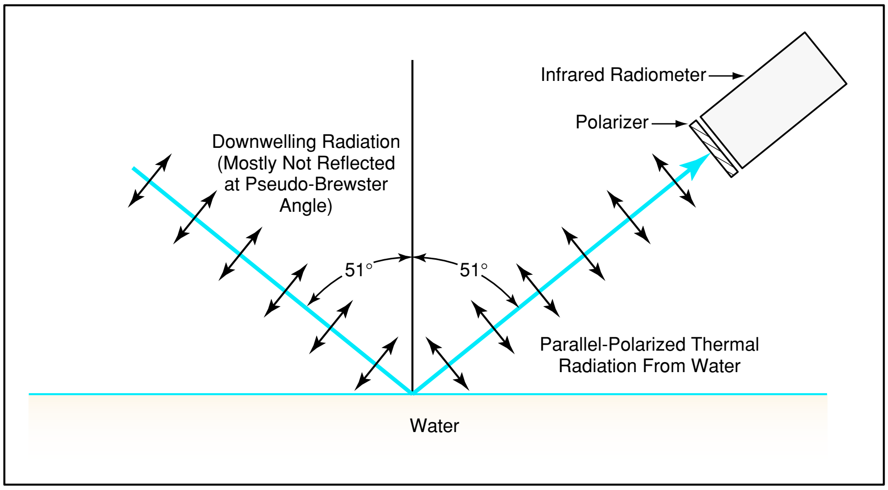

An **Infrared Radiometer** would be aimed toward water at the pseudo-Brewster angle and would respond to radiation polarized parallel (but not perpendicular) to the plane of incidence.

A pseudo-Brewster-angle infrared radiometer has been proposed for use in noncontact measurement of the surface temperature of a large body of water (e.g., a lake or ocean). This radiometer could be situated on a waterborne, airborne, or spaceborne platform.

The design of the pseudo-Brewster-angle radiometer would exploit the spectral-emissivity and polarization characteristics of water to minimize errors attributable to the emissivity of water and to the reflection of downwelling (e.g., Solar and cloud-reflected) infrared radiation. The relevant emissivity and polarization characteristics are the following:

- The Brewster angle is the angle at which light polarized parallel to the plane of incidence on a purely dielectric material is not reflected. The pseudo-Brewster angle, defined for a lossy dielectric (somewhat electrically conductive) material, is the angle for which the reflectivity for parallel-polarized light is minimized. For pure water, the reflectivity for parallel-polarized light is only 2.2×10^{-4} at its pseudo-Brewster angle of 51°. The reflectivity remains near zero, several degrees off from the 51° optimum, allowing this angle of incidence requirement to be easily achieved.
- The wavelength range of interest for measuring water temperatures is 8 to 12 μm. The emissivity of water for parallel-polarized light at the pseudo-Brewster angle is greater than 0.999 in this wavelength range.

The radiometer would be sensitive in the wavelength range of 8 to 12 μm, would be equipped with a polarizer to discriminate against infrared light polarized perpendicular to the plane of incidence, and would be aimed toward a body of water at the pseudo-Brewster angle (see figure). Because the infrared radiation entering the radiometer would be polarized parallel to the plane of incidence and because very little downwelling parallel-polarized radiation would be reflected into the radiometer on account of the pseudo-Brewster arrangement, the radiation received by the radiometer would consist almost entirely of thermal emission from the surface of the water. Because the emissivity of the water would be very close to 1, the water could be regarded as a close approximation of a blackbody for the purpose of computing its surface temperature from the radiometer measurements by use of the Planck radiation law.

This work was done by Robert Ryan, Thomas Nixon, and Mary Pagnutti of Lockheed Martin Corp. and Vicki Zanoni of **Stennis Space Center**.

Inquiries concerning rights for the commercial use of this invention should be addressed to the Intellectual Property Manager, Stennis Space Center [see page 1]. Refer to SSC-00134.

Improved Measurement of Coherence in Presence of Instrument Noise

The coherence function can be measured more accurately by accounting for the effects of instrument noise.

John F. Kennedy Space Center, Florida

A method for correcting measured coherence spectra for the effect of incoherent instrument noise has been developed and demonstrated. Coherence measurements are widely used in engineering and science to determine the extent to which two signals are alike. The signals may come from two different sources or from the same source at different times. The coherence of time-lagged signals from a single source is an excellent indication of the effective lifetime of the signal components as a function of their frequency. Unfortunately, incoherent instrument noise will bias the measurement to lower values and may lead the user of the data to false conclusions about the longevity of significant features.

The new method may be used whenever both the signal and noise power spectra are known and the noise is incoherent both with the signal and with itself at the applicable time delays. It provides a corrected coherence spectrum given the measured coherence and power spectra. For power-law signal spectra and instrumental white noise, the correction formula takes a particularly simple and explicit form. Since many geophysical signals exhibit power-law behavior and most instrument noise spectra approach white noise, the simplified form should be widely applicable in meteorology, oceanography, geology, and planetary geophysics.

The derivation of the method and the resulting formulas for both the general case and the power-law/white-noise case may be found in the Appendix to "The Coherence Time of Mid-Tropospheric Wind Features as a Function of Vertical Scale From 300 m to 2 Km", *Journal of Applied Meteorology*, Vol. 39, pp 2409-2420, December 2000.

This work was done by Francis J. Merceret of **Kennedy Space Center**.

Inquiries concerning rights for the commercial use of this invention should be addressed to the Technology Programs and Commercialization Office, Kennedy Space Center, (321) 867-4879. Refer to KSC-12267.

Compact Instruments Measure Helium-Leak Rates

Compact, lightweight instruments have been developed for measuring small flows of helium and/or detecting helium leaks in solenoid valves when the valves are nominally closed. These instruments do not impede the flows when the valves are nominally open. They can be integrated into newly fabricated valves or retrofitted to previously fabricated valves. Each instrument includes an upstream and a downstream thermistor separated by a heater, plus associated analog and digital heater-control, signal-conditioning, and data-processing circuits. The thermistors and heater are off-the-shelf surface mount components mounted on a circuit board in the flow path. The operation of the instrument is based on a well-established thermal mass-flow-measurement technique: Convection by the flow that one seeks to measure gives rise to transfer of heat from the heater to the downstream thermistor. The temperature difference measured by the thermistors is directly related to the rate of flow. The calibration curve from temperature gradient to helium flow is closely approximated via fifth-order polynomial. A microprocessor that is part of the electronic circuitry implements the calibration curve to compute the flow rate from the thermistor readings.

This work was done by Stephen Stout and Christopher Immer of Dynacs, Inc., for **Kennedy Space Center**.
KSC-12216

Books and Reports

Irreversible Entropy Production in Two-Phase Mixing Layers

This report presents a study of dissipation (irreversible production of entropy) in three-dimensional, temporal mixing layers laden with evaporating liquid drops. The purpose of the study is to examine the effects of evaporating drops on the development of turbulent features in flows. Direct numerical simulations were performed to analyze transitional states of three mixing layers: one without drops, and two that included drops at different initial mass loadings. Without drops, the dissipation is essentially due to viscous effects. It was found that in the presence of drops, the largest contribution to dissipation was made by heating and evaporation of the drops, and that at large length scales, this contribution is positive (signifying that the drops reduce turbulence), while at small scales, this contribution is negative (the drops increase turbulence). The second largest contribution to dissipation was found to be associated with the chemical potential, which leads to an increase in turbulence at large scales and a decrease in turbulence at small scales. The next smaller contribution was found to be that of viscosity. The fact that viscosity effects are only third in order of magnitude in the dissipation is in sharp contrast to the situation for the mixing layer without the drops. The next smaller contribution — that of the drag and momentum of the vapor from the drops — was found to be negative at lower mass loading but to become positive at higher mass loading.

This work was done by Josette Bellan and Nora Okong'o of Caltech for **NASA's Jet Propulsion Laboratory**. *To obtain a copy of the report, "Irreversible entropy production in two-phase flows with evaporating drops," see TSP's [page 1].*
NPO-30586

Subsonic and Supersonic Effects in Bose-Einstein Condensate

A paper presents a theoretical investigation of subsonic and supersonic effects in a Bose-Einstein condensate (BEC). The BEC is represented by a time-dependent, nonlinear Schroedinger equation that includes terms for an external confining potential term and a weak interatomic repulsive potential proportional to the number density of atoms. From this model are derived Madelung equations, which relate the quantum phase with the number density, and which are used to represent excitations propagating through the BEC. These equations are shown to be analogous to the classical equations of flow of an inviscid, compressible fluid characterized by a speed of sound $(g/\rho_0)^{1/2}$, where g is the coefficient of the repulsive potential and ρ_0 is the unperturbed mass density of the BEC. The equations are used to study the effects of a region of perturbation moving through the BEC. The excitations created by a perturbation moving at subsonic speed are found to be described by a Laplace equation and to propagate at infinite speed. For a supersonically moving perturbation, the excitations are found to be described by a wave equation and to propagate at finite speed inside a Mach cone.

This work was done by Michail Zak of Caltech for **NASA's Jet Propulsion Laboratory**. *To obtain a copy of the paper, "Sub- and supersonic effects in Bose-Einstein condensate," see TSP's [page 1].*
NPO-30637

Materials

Hardware, Techniques, and Processes

Nanolaminate Mirrors With "Piston" Figure-Control Actuators

Lightweight adaptive imaging mirrors can be built faster than can heavier glass mirrors.

NASA's Jet Propulsion Laboratory, Pasadena, California

Efforts are under way to develop a special class of thin-shell curved mirrors for high-resolution imaging in visible and infrared light in a variety of terrestrial or extraterrestrial applications. These mirrors can have diameters of the order of a meter and include metallic film reflectors on nanolaminate substrates supported by multiple distributed piezoceramic "piston"-type actuators for micron-level figure control. Whereas conventional glass mirrors of equivalent size and precision have areal mass densities between 50 and 150 kg/m^2, the nanolaminate mirrors, including not only the reflector/shell portions but also the actuators and the backing structures needed to react the actuation forces, would have areal mass densities that may approach ≈5 kg/m^2. Moreover, whereas fabrication of a conventional glass mirror of equivalent precision takes several years, the reflector/shell portion of a nanolaminate mirror can be fabricated in less than a week, and its actuation system can be fabricated in 1 to 2 months.

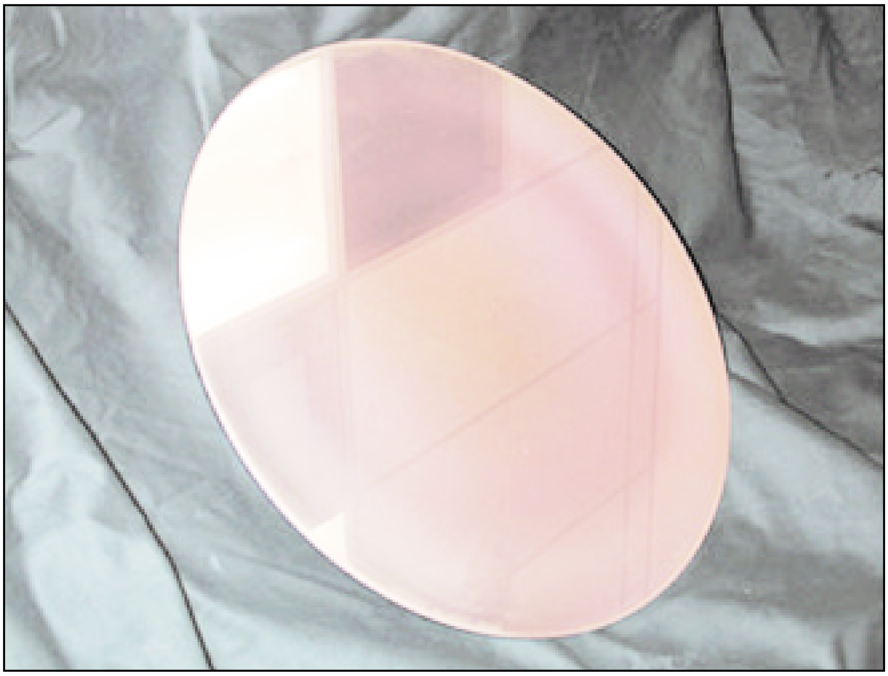

A **Cu/Cu$_x$Zr$_y$ Nanolaminate** was fabricated on a super-polished low-thermal-expansion glass form.

The engineering of these mirrors involves a fusion of the technological heritage of multisegmented adaptive optics and deformable mirrors with more recent advances in metallic nanolaminates and in mathematical modeling of the deflections of thin, curved shells in response to displacements by multiple, distributed actuators. Because a nanolaminate shell is of the order of 10 times as strong as an otherwise identical shell made of a single, high-strength, non-nanolaminate metal suitable for mirror use, a nanolaminate mirror can be made very thin (typically between 100 and 150 μm from the back of the nanolaminate substrate to the front reflecting surface). The thinness and strength of the nanolaminate are what make it possible to use distributed "piston"-type actuators for surface figure control with minimal local concentrated distortion (called print-through in the art) at the actuation points.

Nanolaminate mirror substrates are fabricated in a direct replication process that consists of magnetron sputtering on precise, optical-quality master tools. As a result, the mirror substrates as manufactured (see figure) have nearly optical quality. Because nanolaminates are metals, their coefficients of thermal expansion are greater than those of the low-thermal-expansion glasses ordinarily used to make precise curved mirrors. Hence, backing structures should be made of materials with coefficients of thermal expansion matching those of the nanolaminate mirror shells. The actuators could be used to compensate for any residual thermally induced surface-figure distortions up to a few microns.

This work was done by Andrew Lowman, David Redding, Gregory Hickey, Jennifer Knight, Philip Moynihan, and Shyh-Shiuh Lih of Caltech and Troy Barbee of Lawrence Livermore National Laboratory for **NASA's Jet Propulsion Laboratory**. *Further information is contained in a TSP* *[see page 1].*

NPO-30222

Mixed Conducting Electrodes for Better AMTEC Cells

These electrodes conduct both electrons and sodium cations.

NASA's Jet Propulsion Laboratory, Pasadena, California

Electrode materials that exhibit mixed conductivity (that is, both electronic and ionic conductivity) have been investigated in a continuing effort to improve the performance of the alkali metal thermal-to-electric converter (AMTEC). These electrode materials are intended primarily for use on the cathode side of the sodium-ion-conducting solid electrolyte of a sodium-based AMTEC cell. They may also prove useful in sodium-sulfur batteries, which are under study for use in electric vehicles.

An understanding of the roles played by the two types of conduction in the cathode of a sodium-based AMTEC cell is prerequisite to understanding the advantages afforded by these materials. In a sodium-based AMTEC cell, the anode face of an anode/solid-electrolyte/cathode sandwich is exposed to Na vapor at a suitable pressure. Upon making contact with the solid electrolyte on the anode side, Na atoms oxidize to form Na^+ ions and electrons. Na^+ ions then travel through the electrolyte to the cathode. Na^+ ions leave the electrolyte at the cathode/electrolyte interface and are reduced by electrons that have been conducted through an external electrical load from the anode to the cathode. Once the Na^+ ions have been reduced to Na atoms, they travel through the cathode to vaporize into a volume where the Na vapor pressure is much lower than it is on the anode side. Thus, the cathode design is subject to competing requirements to be thin enough to allow transport of sodium to the low-pressure side, yet thick enough to afford adequate electronic conductivity.

The concept underlying the development of the present mixed conducting electrode materials is the following: The constraint on the thickness of the cathode can be eased by incorporating Na^+-ion-conducting material to facilitate transport of sodium through the cathode in ionic form. At the same time, by virtue of the electronically conducting material mixed with the ionically conducting material, reduction of Na^+ ions to Na atoms can take place throughout the thickness of the cathode. The net effect is to reduce the diffusion and flow resistance to sodium through the electrode while reducing the electronic resistance by providing shorter conduction paths for electrons. Reduced resistance to both sodium transport and electronic conductivity results in an increase in electric power output.

Previous research had shown that mixed-conducting electrodes to improve the performance of an AMTEC cell could be made from mixtures of Mo (an electronic conductor) and Na_2MoO_4 (an ionic conductor) or of W (an electronic conductor) and Na_2WO_4 (an ionic conductor). Unfortunately, electrodes made of these mixtures do not last long: the vapor pressures of Na_2MoO_4 and Na_2WO_4 are so high at the typical operating temperature of a sodium AMTEC cell (between 1,020 and 1,120 K) that these ionically conducting materials evaporate within a few hundred hours of operation.

The present mixed-conducting electrode materials are mixtures of Mo (as before, an electronic conductor) and Na_xTiO_2 (a conductor of both electrons and Na^+ ions). Na_xTiO_2 can be formed by exposing TiO_2 to Na vapor at a temperature >900 °C. Na_xTiO_2 is a mixture of Na-Ti-O compounds, all of which are electronically conducting by virtue of the conductivity of TiO_2, and ionically conducting toward Na^+ ions. In an experiment, an electrode made from a mixture of equal weight proportions of Mo and TiO_2 was found to perform well at a temperature of 830 °C (1,103 K) for >1,000 hours, with no significant change in either electrode power or transport properties. Moreover, the performance of this electrode was found to equal or exceed the performance of the best previously known AMTEC electrode, which was made of RhW.

This work was done by Margaret Ryan, Roger Williams, Margie Homer, and Liana Lara of Caltech for **NASA's Jet Propulsion Laboratory**. *Further information is contained in a TSP [see page 1].*
NPO-20920

Process for Encapsulating Protein Crystals

Crystals can be grown in forms suitable for x-ray diffraction studies.

Lyndon B. Johnson Space Center, Houston, Texas

A process for growing protein crystals encapsulated within membranes has been invented. This process begins with the encapsulation of a nearly saturated aqueous protein solution inside semipermeable membranes to form microcapsules. The encapsulation is effected by use of special formulations of a dissolved protein and a surfactant in an aqueous first liquid phase, which is placed into contact with a second, immiscible liquid phase that contains one or more polymers that are insoluble in the first phase. The second phase becomes formed into the semipermeable membranes that surround microglobules of the first phase, thereby forming the microcapsules. Once formed, the microcapsules are then dehydrated osmotically by exposure to a concentrated salt or polymer solution. The dehydration forms supersaturated solutions inside the microcapsules, thereby enabling nucleation and growth of protein crystals inside the microcapsules.

By suitable formulation of the polymer or salt solution and of other physical and chemical parameters, one can control the rate of transport of water out of the microcapsules through the membranes and thereby create physicochemical conditions that favor the growth, within each microcapsule, of one or a few large crystals suitable for analysis by x-ray diffraction. The membrane polymer can be formulated to consist of low-molecular-weight molecules that do not interfere with the x-ray diffraction analysis of the encapsulated crystals. During dehydration, an electrostatic field can be applied to exert additional control over the rate of dehydration.

This protein-crystal-encapsulation process is expected to constitute the basis of protein-growth experiments to be performed on the space shuttle and the International Space Station. As envisioned, the experiments would involve the exposure of immiscible liquids to each other in sequences of steps under microgravitational conditions. The experiments are expected to contribute to knowledge of the precise conditions under which protein crystals form. By enhancing the ability to grow crystals suitable for x-ray diffraction analysis, this knowledge can be expected to benefit not only the space program but also medicine and the pharmaceutical industry.

The prior art in osmotic dehydration for growing protein crystals involves the use of a small chamber in which a planar reverse-osmosis membrane is positioned between the mother liquor and a dehydrating salt solution. The prior art entails several disadvantages: (1) The nucleation and subsequent growth of protein crystals depend on increasing the concentration of precipitant and protein in the mother liquor; (2) there is no control over the effects of solute-driven convection on the surface of the crystal; (3) the crystals are not protected by any enclosure and thus are subject to physical damage as they are harvested and mounted; and (4) in some instances in the prior art, protein crystals have been protected by mounting them in aqueous gels, but this practice gives rise to the additional (as yet unsolved) problem of removing the gel material without adversely affecting the integrity of the protein crystals.

In contrast, the encapsulation of protein crystals in semipermeable membranes in the present process does not involve the use of gel, yet it creates closed environments that favor the growth of the crystals under prescribed conditions of controlled dehydration and protects the crystals against harsh environments that could otherwise damage the crystals.

In the present protein-crystal-encapsulation process, the microcapsules are spherical. The entire outer surface of the membrane of a microcapsule is accessible for osmotic dewatering as well as for and infiltration by hydrogen or hydroxyl ions. Such infiltration can be utilized to change the pH levels within microcapsules to favor or enhance protein saturation and subsequent crystal growth. The increase (relative to the prior art) in interfacial surface area occasioned by the transition from planar membranes to spherical microcapsules makes it possible to change conditions more rapidly throughout the mother liquor surrounding the crystal(s), thereby promoting the formation of more ordered and more nearly perfect crystals.

This work was done by Dennis R. Morrison of **Johnson Space Center** *and Benjamin Mosier of the Institute for Research, Inc. Further information is contained in a TSP [see page 1].*

This invention is owned by NASA, and a patent application has been filed. Inquiries concerning nonexclusive or exclusive license for its commercial development should be addressed to the Patent Counsel, Johnson Space Center, (281) 483-0837. Refer to MSC-22936.

Lightweight, Self-Deployable Wheels

Compacted, frozen wheels are deployed by heating above T_g.

NASA's Jet Propulsion Laboratory, Pasadena, California

Ultra-lightweight, self-deployable wheels made of polymer foams have been demonstrated. These wheels are an addition to the roster of cold hibernated elastic memory (CHEM) structural applications. Intended originally for use on nanorovers (very small planetary-exploration robotic vehicles), CHEM wheels could also be used for many commercial applications, such as in toys.

The CHEM concept was reported in "Cold Hibernated Elastic Memory (CHEM) Expandable Structures" (NPO-20394), *NASA Tech Briefs*, Vol. 23, No. 2 (February 1999), page 56. To recapitulate: A CHEM structure is fabricated from a shape-memory polymer (SMP) foam. The structure is compressed to a very small volume while in its rubbery state above its glass-transition temperature (T_g). Once compressed, the structure can be cooled below T_g to its glassy state. As long as the temperature remains $<T_g$ the structure remains compacted (in a cold hibernated state), even when the external compressive forces are removed. When the structure is subsequently heated above T_g, it returns to the rubbery state, in which a combination of elasticity and the SMP effect cause it to expand (deploy) to its original size and shape. Once thus deployed, the CHEM structure can be rigidified by cooling below T_g to the glassy state. The structure could be subsequently reheated above T_g and recompacted. The compaction/deployment/rigidification cycle could be repeated as many times as needed.

SMPs with T_gs ranging from –100 to almost +100 °C are available. Hence, it should be possible to select SMPs with T_gs suitable for CHEM structures for a variety of potential terrestrial and outer-space applications. During an investigation directed toward extending the CHEM concept to wheels, several wheel designs for a prototype nanorover were evaluated. CHEM models of the designs were fabricated and assessed by subjecting the models to a CHEM processing cycle. All wheels recovered completely after the cycle, and a wheel design with the fastest deployment was selected for the nanorover. Full-scale wheels were fabricated and assembled on two-wheeled prototype nanorover. Finally, the compacted wheels were successfully deployed at 80 °C and subsequently rigidified, both at room temperature in the terrestrial atmosphere and at a lower temperature and pressure chosen to simulate the Mars atmosphere.

This work was done by Artur Chmielewski, Witold Sokolowski, and Peter Rand of Caltech for **NASA's Jet Propulsion Laboratory**. *Further information is contained in a TSP [see page 1].*
NPO-21225

Grease-Resistant O Rings for Joints in Solid Rocket Motors

There is a continuing effort to develop improved O rings for sealing joints in solid-fuel rocket motors. Following an approach based on the lessons learned in the explosion of the space shuttle *Challenger*, investigators have been seeking O-ring materials that exhibit adequate resilience for effective sealing over a broad temperature range: What are desired are O rings that expand far and fast enough to maintain seals, even when metal sealing surfaces at a joint move slightly away from each other shortly after ignition and the motor was exposed to cold weather before ignition. Other qualities desired of the improved O rings include adequate resistance to ablation by hot rocket gases and resistance to swelling when exposed to hydrocarbon-based greases used to protect some motor components against corrosion. Five rubber formulations — two based on a fluorosilicone polymer and three based on copolymers of epichlorohydrin with ethylene oxide — were tested as candidate O-ring materials. Of these, one of the epichlorohydrin/ethylene oxide formulations was found to offer the closest to the desired combination of properties and was selected for further evaluation.

This work was done by Albert R. Harvey and Harold Feldman (deceased) of Thiokol Propulsion for **Marshall Space Flight Center**. *To obtain a copy of the report, "Resilient, Hydrocarbon Base Grease Resistant O-ring Seals for Solid Rocket Motor Applications," please contact the company at (435) 863-4123.*
MFS-31643

Computer Programs

Electronic Systems

LabVIEW Serial Driver Software for an Electronic Load

A LabVIEW-language computer program enables monitoring and control of a Transistor Devices, Inc., Dynaload WCL232 (or equivalent) electronic load via an RS-232 serial communication link between the electronic load and a remote personal computer. (The electronic load can operate at constant voltage, current, power consumption, or resistance.) The program generates a graphical user interface (GUI) at the computer that looks and acts like the front panel of the electronic load. Once the electronic load has been placed in remote-control mode, this program first queries the electronic load for the present values of all its operational and limit settings, and then drops into a cycle in which it reports the instantaneous voltage, current, and power values in displays that resemble those on the electronic load while monitoring the GUI images of pushbuttons for control actions by the user. By means of the pushbutton images and associated prompts, the user can perform such operations as changing limit values, the operating mode, or the set point. The benefit of this software is that it relieves the user of the need to learn one method for operating the electronic load locally and another method for operating it remotely via a personal computer.

This program was written by Vincent Scullin of **Glenn Research Center** *and Christopher Garcia of QSS Group, Inc. Further information is contained in a TSP [see page 1].*

Inquiries concerning rights for the commercial use of this invention should be addressed to NASA Glenn Research Center, Commercial Technology Office, Attn: Steve Fedor, Mail Stop 4–8, 21000 Brookpark Road, Cleveland, Ohio 44135. Refer to LEW-17292.

Fabrication Technology

Software Computes Tape-Casting Parameters

Tcast2 is a FORTRAN computer program that accelerates the setup of a process in which a slurry containing metal particles and a polymeric binder is cast, to a thickness regulated by a doctor blade, onto fibers wound on a rotating drum to make a "green" precursor of a metal-matrix/fiber composite tape. Before Tcast2, setup parameters were determined by trial and error in time-consuming multiple iterations of the process. In Tcast2, the fiber architecture in the final composite is expressed in terms of the lateral distance between fibers and the thickness-wise distance between fibers in adjacent plies. The lateral distance is controlled via the manner of winding. The interply spacing is controlled via the characteristics of the slurry and the doctor-blade height. When a new combination of fibers and slurry is first cast and dried to a green tape, the shrinkage from the wet to the green condition and a few other key parameters of the green tape are measured. These parameters are provided as input to Tcast2, which uses them to compute the doctor-blade height and fiber spacings needed to obtain the desired fiber architecture and fiber volume fraction in the final composite.

This program was written by Henry C. de Groh III of **Glenn Research Center**. *Further information is contained in a TSP [see page 1].*

Inquiries concerning rights for the commercial use of this invention should be addressed to NASA Glenn Research Center, Commercial Technology Office, Attn: Steve Fedor, Mail Stop 4–8, 21000 Brookpark Road, Cleveland, Ohio 44135. Refer to LEW-17323.

Mathematics and Information Sciences

Software for Tracking Costs of Mars Projects

The Mars Cost Tracking Model is a computer program that administers a system set up for tracking the costs of future NASA projects that pertain to Mars. Previously, no such tracking system existed, and documentation was written in a variety of formats and scattered in various places. It was difficult to justify costs or even track the history of costs of a spacecraft mission to Mars. The present software enables users to maintain all cost-model definitions, documentation, and justifications of cost estimates in one computer system that is accessible via the Internet. The software provides sign-off safeguards to ensure the reliability of information entered into the system. This system may eventually be used to track the costs of projects other than only those that pertain to Mars.

This program was written by Alvin Wong and Keith Warfield of Caltech for **NASA's Jet Propulsion Laboratory**. *Further information is contained in a TSP [see page 1].*

This software is available for commercial licensing. Please contact Don Hart of the California Institute of Technology at (818) 393-3425. Refer to NPO-30365.

Software for Replicating Data Between X.500 and LDAP Directories

X500/LDAP Directory Replication Utility is a computer program for replicating information between X.500 and LDAP directories. [X.500 is an international standard for on-line directory services. LDAP (Lightweight Directory Access Protocol) is a simple directory access protocol.] The utility can be used to replicate an object of any type from X.500 to LDAP or from LDAP to X.500. The program uses the LDAP version 2 protocol, which is capable of working with both X.500 and LDAP directories. The program can provide any or all of the following services: (1) replicate only modified objects; (2) force replication of all objects; (3) replicate individual objects, one level of objects, or a subtree of objects; (4) filter sets of objects to select ones to be replicated; (5) remove and/or modify object classes from objects that are replicated; and (6) select and/or limit attributes that are replicated. The program includes a separate program that is used to remove objects that are no longer required to be replicated.

This program was written by Thomas Wolfe of Caltech for **NASA's Jet Propulsion Laboratory**. *Further information is contained in a TSP [see page 1].*

This software is available for commercial licensing. Please contact Don Hart of the California Institute of Technology at (818) 393-3425. Refer to NPO-30430.

The Technical Work Plan Tracking Tool

The Technical Work Plan Tracking Tool is a web-based application that enables interactive communication and approval of contract requirements that pertain to the administration of the Science, Engineering, Analysis, and Test (SEAT) contract at

Johnson Space Center. The implementation of the application has (1) shortened the Technical Work Plan approval process, (2) facilitated writing and documenting requirements in a performance-based environment with associated surveillance plans, (3) simplified the contractor's estimate of the cost for the required work, and (4) allowed for the contractor to document how they plan to accomplish the work. The application is accessible to over 300 designated NASA and contractor employees via two Web sites. For each employee, the application regulates access according to the employee's authority to enter, view, and/or print out diverse information, including reports, work plans, purchase orders, and financial data. Advanced features of this application include on-line approval capability, automatic e-mail notifications requesting review by subsequent approvers, and security inside and outside the firewall.

This program was designed by Cinda Chullen, Adele Leighton, Richard A. Weller, and Jared Woodfill of **Johnson Space Center***, and William E. Parkman, Glenn L. Ellis, and Marilyn M. Wilson of Lockheed Martin Corp., and developed by Nina S. Johnson and William E. Moody of Lockheed Martin Corp. Further information is contained in a TSP [see page 1].*
MSC-23361

Mechanics

Hardware, Techniques, and Processes

Books and Reports

Improved Multiple-DOF SAW Piezoelectric Motors

Actuators without bearings or lead screws could be integrated into mechanisms and structures.

NASA's Jet Propulsion Laboratory, Pasadena, California

Surface-acoustic-wave (SAW) piezoelectric motors of a proposed type would be capable of operating in multiple degrees of freedom (DOFs) simultaneously and would be amenable to integration into diverse structures and mechanisms. These motors would be compact and structurally simple and would not contain bearings or lead screws. One example of a particularly useful motor of this type would be a two-dimensional-translation stage. Another such example would be a self-actuated spherical joint that could be made to undergo controlled, simultaneous rotations about two orthogonal axes: Such a motor could serve as a mechanism for aiming an "eyeball" camera or as a compact transducer in, and an integral part of, a joint in a robot arm.

The multiple-DOF SAW piezoelectric motors as now proposed would be successors to the ones reported in "Multiple-DOF Surface-Acoustic-Wave Piezoelectric Motors" (NPO-20735), *NASA Tech Briefs*, Vol. 24, No. 12 (December 2000), page 5b. The basic principle of operation of a multiple-DOF SAW piezoelectric motor is a straightforward extension of that of single-DOF SAW piezoelectric motors, which have been reported in several previous *NASA Tech Briefs* articles: For example, in the case of a linear SAW piezoelectric motor, piezoelectric transducers at opposite ends of a stator excite surface acoustic waves that travel along the surface of the stator. An object (denoted the slider) is pressed against the stator with sufficient pressure (in practice ≈300 MPa) that it remains in frictional contact with the stator at all times. The slider rides the crests of the waves and is thereby made to move along the surface of the stator. The direction of motion (forward or backward) is controlled by selecting the relative phase of waves generated by the two piezoelectric transducers. The speed increases with the amplitude of the waves and thus with the magnitude of the voltage applied to the transducers.

The extension of this actuation principle to multiple degrees of freedom can be illustrated via the example of a two-dimensional-translation stage as now proposed (see Figure 1). In this case, the slider would be clamped between an upper and a lower stator and there would be two pairs of SAW piezoelectric transducers (instead of a single pair) on each stator. Small bosses on the upper and lower surfaces of the slider would make contact with the upper and lower stators, respectively. The pairs of transducers would be oriented orthogonally so that they could generate orthogonally propagating waves, making it possible to move the slider along either of two orthogonal axes. Like other SAW piezoelectric motors, a motor as now proposed would hold its position when not energized because the static friction generated by the clamping force would act as a braking force.

The ability of a surface acoustic wave to travel on a curved surface would make it possible to design a spherical 2-DOF SAW actuator like that depicted in Figure 2. In this

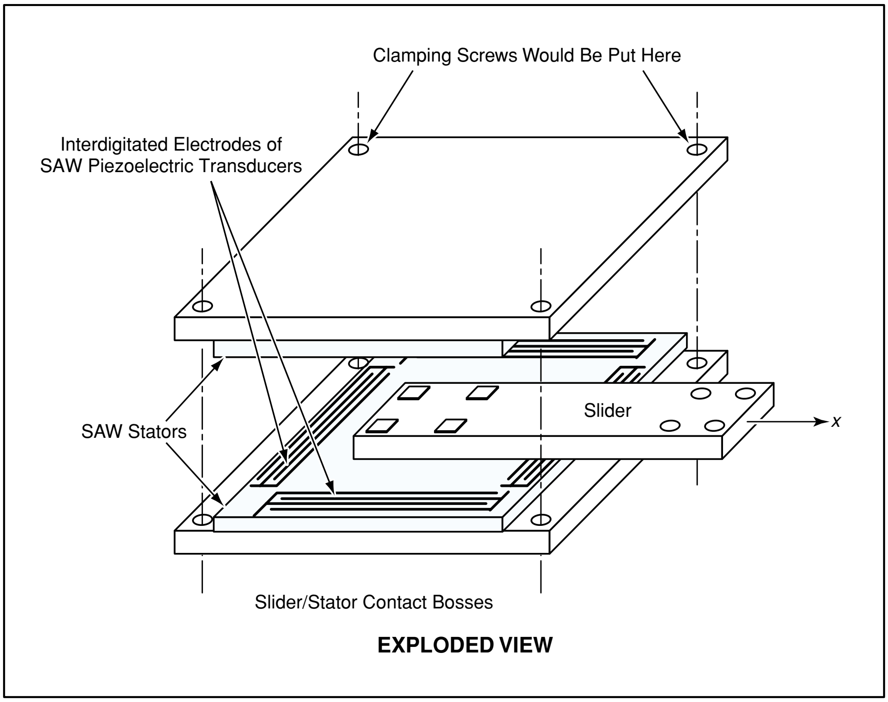

Figure 1. In this **Two-Dimensional-Translation Stage** the slider would move along the *x* or *y* direction when *x*- or *y*-propagating surface acoustic waves were excited in the stators.

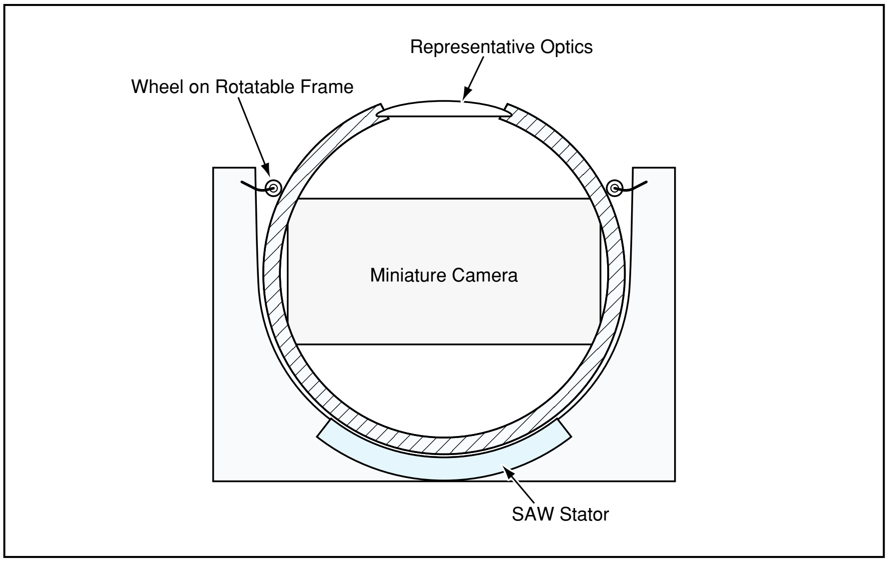

Figure 2. The **Sphere Would Rotate** about either of two orthogonal horizontal axes when surface acoustic waves were excited in the stator by use of either of two orthogonal pairs of SAW piezoelectric transducers in the stator.

case, two pairs of SAW piezoelectric transducers would be oriented orthogonally on a concave spherical stator instead of a flat stator, and the slider would be a sphere of nearly equal radius pressed against the stator.

In general, the minimum actuation step size would be approximately inversely proportional to the SAW excitation frequency. At contemplated maximum excitation frequencies of the order of tens of megahertz, minimum step sizes of nanometers could be achieved. Another advantage of using high excitation frequencies is that it would make it possible to achieve high force densities, thereby enabling the design of relatively small, lightweight actuators.

This work was done by Yoseph Bar-Cohen, Xiaoqi Bao, Anthony Hull, and John Wright of Caltech for **NASA's Jet Propulsion Laboratory**. *Further information is contained in a TSP [see page 1].*

In accordance with Public Law 96-517, the contractor has elected to retain title to this invention. Inquiries concerning rights for its commercial use should be addressed to

Intellectual Assets Office
JPL
Mail Stop 202-233
4800 Oak Grove Drive
Pasadena, CA 91109
(818) 354-2240
E-mail: ipgroup@jpl.nasa.gov

Refer to NPO-20859, volume and number of this NASA Tech Briefs *issue, and the page number.*

Propulsion Flight-Test Fixture

Subscale engines can be flight-tested early in the development cycle.

Dryden Flight Research Center, Edwards, California

Figure 1. The **PFTF Holds the Test Article** underneath the F-15B airplane during flight.

NASA Dryden Flight Research Center's new Propulsion Flight Test Fixture (PFTF), designed in house, is an airborne engine-testing facility that enables engineers to gather flight data on small experimental engines. Without the PFTF, it would be necessary to obtain such data from traditional wind tunnels, ground test stands, or laboratory test rigs.

Traditionally, flight testing is reserved for the last phase of engine development. Generally, engines that embody new propulsion concepts are not put into flight environments until their designs are mature: in such cases, either vehicles are designed around the engines or else the engines are mounted in or on missiles. However, a "captive carry" capability of the PFTF makes it possible to test engines that feature air-breathing designs (for example, designs based on the rocket-based combined cycle) economically in subscale experiments.

The discovery of unknowns made evident through flight tests provides valuable information to engine designers early in development, before key design decisions are made, thereby potentially affording large benefits in the long term. This is especially true in the transonic region of flight (from mach 0.9 to around 1.2), where it can be difficult to obtain data from wind tunnels and computational fluid dynamics.

In January 2002, flight-envelope expansion to verify the design and capabilities of the PFTF was completed. The PFTF was flown on a specially equipped supersonic F-15B research testbed airplane, mounted on the airplane at a center-line attachment fixture, as shown in Figure 1.

NASA's F-15B testbed has been used for several years as a flight-research platform. Equipped with extensive research air-data, video, and other instrumentation systems, the airplane carries externally mounted test articles. Traditionally, the majority of test articles flown have been mounted at the center-line tank-attachment fixture, which is a hardpoint (essentially, a standardized weapon-mounting fixture). This hardpoint has large weight margins, and, because it is located near the center of gravity of the airplane, the weight of equipment mounted there exerts a minimal effect on the stability and controllability of the airplane.

The PFTF (see Figure 2) includes a one-piece aluminum structure that contains space for instrumentation, propellant tanks, and feed-system components. The PFTF also houses a force balance, on which is mounted the subscale engine or other experimental apparatus that is to be the subject of a flight test. The force balance measures a combination of inertial and aerodynamic forces and moments acting on the experimental apparatus.

The PFTF instrumentation system is a slave to the instrumentation system of the F-15B airplane. At present, as many as 128 parameters can be monitored by use of the PFTF; however, it is possible to expand the capabilities of the PFTF to monitor more parameters, if necessary. These monitored parameters can include, but are not limited to, pressures, temperatures, accelerations, vibrations, and strains. Sample rates are variable, generally between 10 and 400 samples per second, but much higher data-acquisition rates are possible. Parameters can be recorded aboard the F-15B airplane by use of a digital recorder or telemetered to a control room.

An experimental apparatus as heavy as 500 lb (≈227 kg) and as long as 12 ft (≈3.7 m) can be mounted on the PFTF. The PFTF can accommodate experiments in which are produced thrusts or drags as large as 2,000 lb (≈8.9 kN) and side forces up to 500 lb (≈2.2 kN). For envelope-expansion

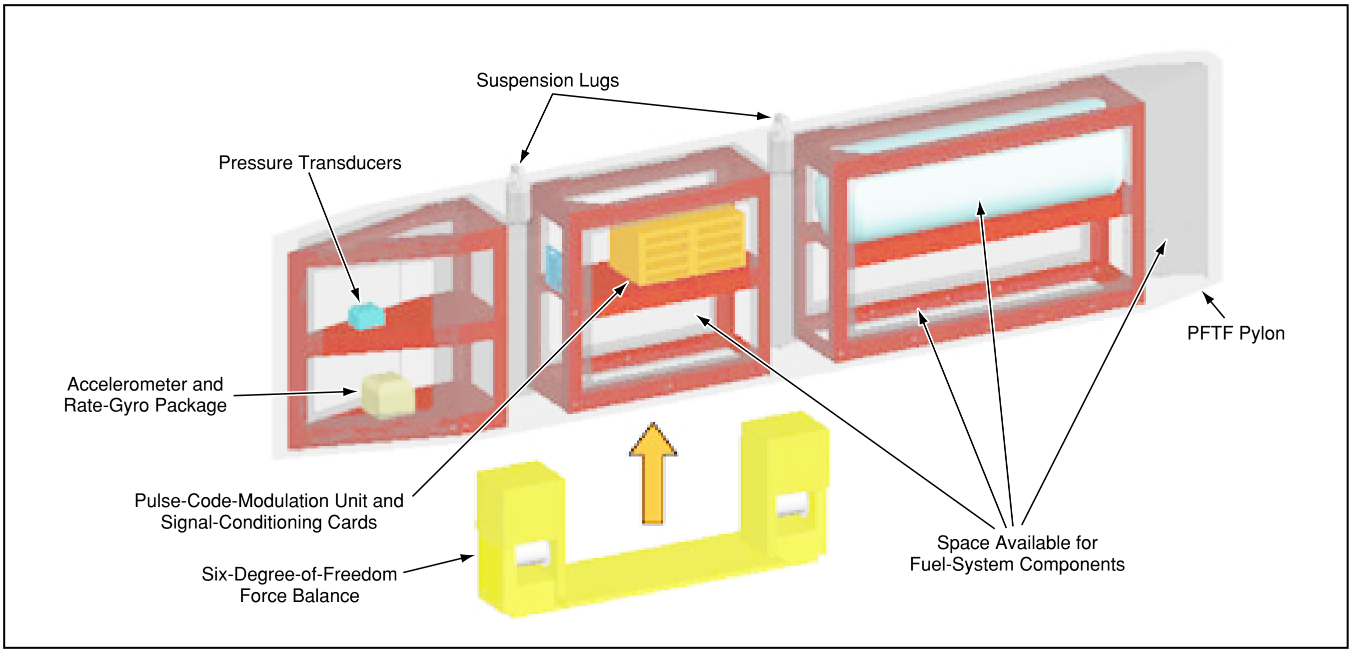

Figure 2. The **Interior of the PFTF** accommodates instrumentation and fuel-system hardware needed for an experiment.

flights, a surrogate engine-shape body denoted the cone drag experiment was flown attached to the force balance. The cone drag experiment inertially and spatially approximated a large engine test article. This cone drag experiment produced drag forces of up to 1,400 lb (≈6.2 kN) at high speeds. A top speed of mach 2.0 and a dynamic pressure of 1,100 psf (≈53 kPa) were attained in this configuration.

This work was done by Nate Palumbo, M. Jake Vachon, Dave Richwine, and Tim Moes of ***Dryden Flight Research Center*** *and Gray Creech of AS&M. Further information is contained in a TSP [see page 1].*
DRC-02-23

Mechanical Amplifier for a Piezoelectric Transducer

In addition to multiplication of stroke, the design affords momentum compensation.

NASA'S Jet Propulsion Laboratory, Pasadena, California

A mechanical amplifier has been devised to multiply the stroke of a piezoelectric transducer (PZT) intended for use at liquid helium temperatures. Interferometry holds the key to high angular resolution imaging and astrometry in space. Future space missions that will detect planets around other solar systems and perform detailed studies of the evolution of stars and galaxies will use new interferometers that observe at mid- and far-infrared wavelengths. Phase-measurement interferometry is key to many aspects of astronomical interferometry, and PZTs are ideal modulators for most methods of phase measurement, but primarily at visible wavelengths. At far infrared wavelengths of 150 to 300 μm, background noise is a severe problem and all optics must be cooled to about 4 K. Under these conditions, piezos are ill-suited as modulators, because their throw is reduced by as much as a factor of 2, and even a wavelength or two of modulation is beyond their capability. The largest commercially available piezo stacks are about 5 in. (12.7 cm) long and have a throw of about 180 μm at room temperature and only 90 μm at 4 K. It would seem difficult or impossible to use PZTs for phase measurements in the far infrared were it not for the new mechanical amplifier that was designed and built.

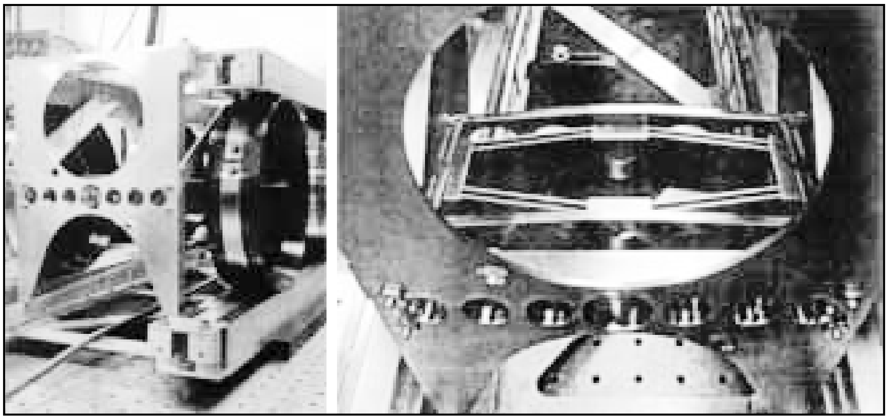

A **Four-Bar Linkage** provides stroke amplification and momentum compensation for the PZT mounted inside it.

To compensate for the loss of travel at cryogenic temperatures, the PZT is mounted in a novel mechanical amplifier that supports one of the mirrors of the interferometer. The mechanical amplifier, shown in the figure, was designed based on an original concept at JPL dating from 1993. The mechanical amplifier resembles an elongated parallelogram with pairs of parallel flexures along each side. The PZT is compressed along the axis of the long diagonal of the parallelogram by support flexures at each end. The expansion of the PZT along the long diagonal causes the ends of the short diagonal to move towards each with a motion amplified by a factor of 3 or 4. The parallel flexures are used to eliminate unwanted twisting and vibration modes such that a small mirror will not tilt when translated by the amplifier. The support flexures that hold the PZT allow a symmetrical expansion of the piezo within the amplifier. The amplifier is designed to be completely symmetric and balanced such that inertia forces are nulled. This provides mechanical stability that allows rapid (100-Hz) sampling without inducing vibrations. Optical interferometers normally obtain the mechanical stability and momentum compensation by using an additional piezo stack mounted back-to-back with the first piezo so that the second one has motions that are equal but opposite in direction. By mounting the stack symmetrically with the support flexures the stack expands equally about its center, does not induce vibrations, and does not require momentum compensation.

This new mechanical amplifier provides both a longer stroke for standard piezo stacks and the necessary mechanical stability through an ingenious mounting arrangement. The device is made of titanium and machined using a wire EDM (electrical-discharge machining) process so as to be as strong and lightweight as possible. It is compact using only a single piezo stack, making it ideally suited for phase-measurement in a cryogenic environment.

This work was done by James Moore, Mark Swain, Peter Lawson, and Robert Calvet of Caltech for **NASA's Jet Propulsion Laboratory**. *Further information is contained in a TSP [see page 1].*
NPO-30289

Swell Sleeves for Testing Explosive Devices

A device is detonated in a sleeve and the resultant swelling is measured.

Lyndon B. Johnson Space Center, Houston, Texas

A method of testing explosive and pyrotechnic devices involves exploding the devices inside swell sleeves. Swell sleeves have been used previously for measuring forces. In the present method, they are used to obtain quantitative indications of the energy released in explosions of the devices under test.

A swell sleeve is basically a thick-walled, hollow metal cylinder threaded at one end to accept a threaded surface on a device to be tested (see Figure 1). Once the device has been tightly threaded in place in the swell sleeve, the device-and-swell-sleeve assembly is placed in a test fixture, then the device is detonated.

After the explosion, the assembly is removed from the test fixture and placed in a coordinate-measuring machine for measurement of the diameter of the swell sleeve as a function of axial position. For each axial position, the original diameter of the sleeve is subtracted from the diameter of the sleeve as swollen by the explosion to obtain the diametral swelling as a function of axial position (see Figure 2). The amount of swelling is taken as a measure of the energy released in the explosion. The amount of swelling can be compared to a standard amount of swelling to determine whether the pyrotechnic device functioned as specified.

This work was done by Todd J. Hinkel, Richard J. Dean, Carl W. Hohmann, Scott C. Hacker, and Douglas W. Harrington of **Johnson Space Center** *and James W. Bacak of Lockheed Engineering and Sciences Co. Further information is contained in a TSP [see page 1].*
MSC-23306

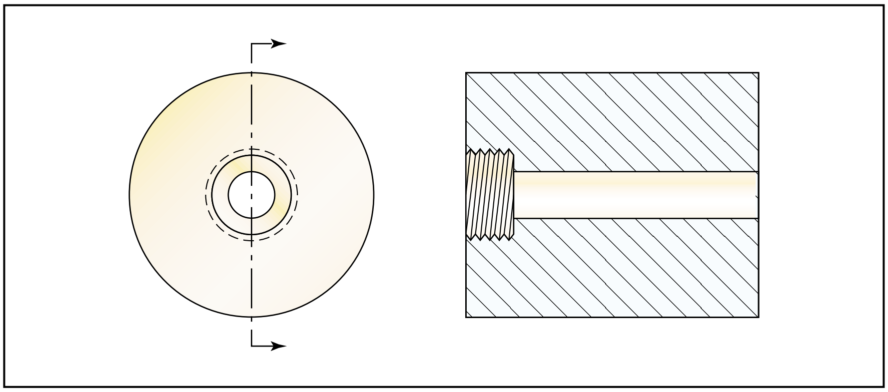

Figure 1. A **Swell Sleeve** is designed and fabricated to accept an explosive device. It is so named because its wall is thick enough not to burst yet thin enough to swell measurably when the device is exploded within it.

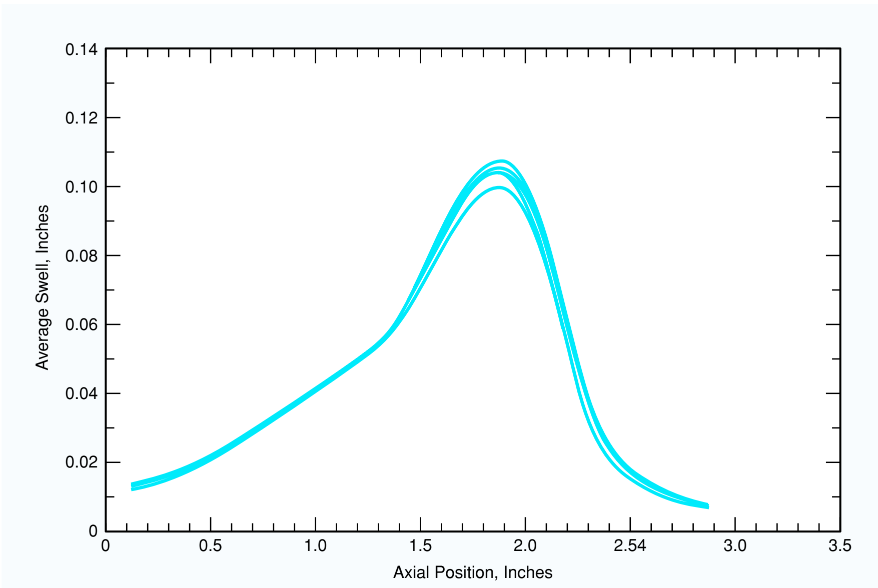

Figure 2. These **Diametral Swells** as functions of axial position were obtained in swell-sleeve tests of explosive devices used to separate an external-tank assembly from a space shuttle.

Linear Back-Drive Differentials

Lighter, smaller, simpler alternatives to gear differentials would be used in limited-rotation applications.

NASA's Jet Propulsion Laboratory, Pasadena, California

Linear back-drive differentials have been proposed as alternatives to conventional gear differentials for applications in which there is only limited rotational motion (e.g., oscillation). The finite nature of the rotation makes it possible to optimize a linear back-drive differential in ways that would not be possible for gear differentials or other differentials that are required to be capable of unlimited rotation. As a result, relative to gear differentials, linear back-drive differentials could be more compact and less massive, could contain fewer complex parts, and could be less sensitive to variations in the viscosities of lubricants.

Linear back-drive differentials would operate according to established principles of power ball screws and linear-motion drives, but would utilize these principles in an innovative way. One major characteristic of such mechanisms that would be exploited in linear back-drive differentials is the possibility of designing them to drive or back-drive with similar efficiency and energy input: in other words, such a mechanism can be designed so that a rotating screw can drive a nut linearly or the linear motion of the nut can cause the screw to rotate.

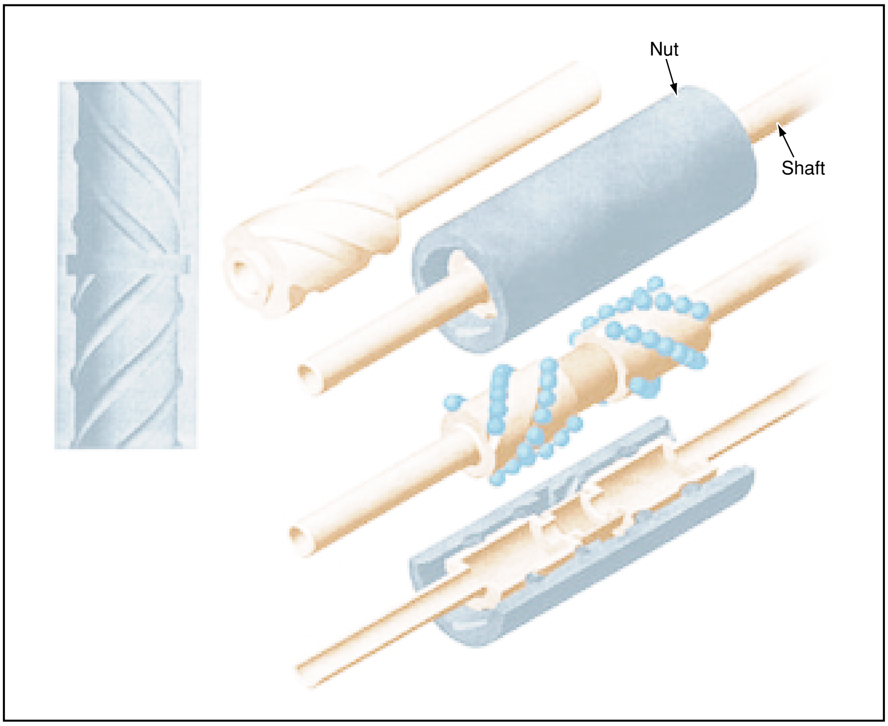

A **Linear Back-Drive Differential** would incorporate components like those of ball screws and linear-motion drives.

A linear back-drive differential (see figure) would include two collinear shafts connected to two parts that are intended to engage in limited opposing rotations. The linear back-drive differential would also include a nut that would be free to translate along its axis but not to rotate. The inner surface of the nut would be right-hand threaded at one end and left-hand threaded at the opposite end to engage corresponding right- and left-handed threads on the shafts. A rotation and torque introduced into the system via one shaft would drive the nut in linear motion. The nut, in turn, would back-drive the other shaft, creating a reaction torque. Balls would reduce friction, making it possible for the shaft/nut coupling on each side to operate with 90 percent efficiency.

This work was done by Peter Waydo of Caltech for **NASA's Jet Propulsion Laboratory**. *Further information is contained in a TSP [see page 1].*

NPO-30366

Miniature Inchworm Actuators Fabricated by Use of LIGA

These MEMS actuators could be mass-produced at low unit cost.

NASA's Jet Propulsion Laboratory, Pasadena, California

Miniature inchworm actuators that would have relatively simple designs have been proposed for applications in which there are requirements for displacements of the order of microns or tens of microns and for the ability to hold their positions when electric power is not applied. The proposed actuators would be members of the class of microelectromechanical systems (MEMS), but would be designed and fabricated following an approach that is somewhat unusual for MEMS.

Like other MEMS actuators, the proposed inchworm actuators could utilize thermoplastic, bimetallic, shape-memory-alloy, or piezoelectric actuation principles. The figure depicts a piezoelectric inchworm actuator according to the proposal. As in other inchworm actuators, linear motion of an extensible member would be achieved by lengthening and shortening the extensible member in synchronism with alternately clamping and releasing one and then the other end of the member. In this case, the moving member would be the middle one; the member would be piezoelectric and would be shortened by applying a voltage to it. The two outer members would also be piezoelectric; the release of the clamps on the upper or lower end would be achieved by applying a voltage to the electrodes on the upper or lower ends, respectively, of these members.

Usually, MEMS actuators cannot be fabricated directly on the side walls of silicon wafers, yet the geometry of this actuator necessitates such fabrication. The solution, according to the proposal, would be to use the microfabrication technique known by the German acronym LIGA — "lithographie, galvanoformung, abformung," which means lithography, electroforming, molding. LIGA involves x-ray lithography of a polymer film followed by selective removal of material to form a three-dimensional pattern from which

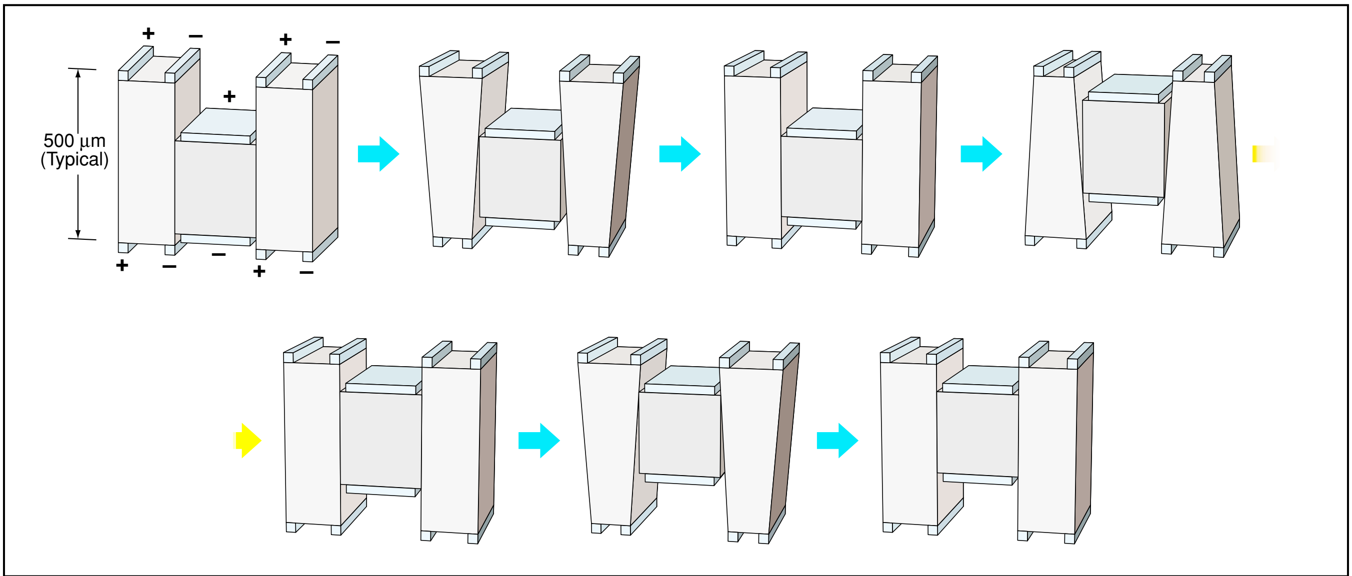

A **Miniature Piezoelectric Inchworm Actuator** fabricated by use of LIGA according to the proposal would have a geometry considerably simpler than that of prior inchworm actuators conventionally assembled from discrete parts.

a mold is made. Among the advantages of LIGA for this purpose are that it is applicable to a broad range of materials, can be used to implement a variety of designs, including those of structures >1 mm high, affords submicron precision, and is amenable to mass production at relatively low unit cost.

Fabrication of the proposed actuators would involve some technological risks — in particular, in the integration of electrode connection lines and placement of actuator elements. It will also be necessary to perform an intensive study of the feasibility of growing piezoelectric crystals onto LIGA molds.

This work was done by Eui-Hyeok Yang of Caltech for **NASA's Jet Propulsion Laboratory**. *Further information is contained in a TSP [see page 1].*
NPO-30429

Books and Reports

Using ERF Devices To Control Deployments of Space Structures

A report proposes devices containing electrorheological fluids (ERFs) damper for controlling deployments of lightweight, flexible structures in outer space. The structures would include spring members that could be wound or compressed for compact stowage during transport. The ERF based damper would keep the structures compacted and/or regulate the speeds with which the structures would spring out for deployment. After deployment, ERF based dampening mechanism could be used to rigidize the structures or damp their vibrations. An experimental ERF deployment controlled structure described in the report comprised two metal carpenter's measuring tapes sandwiched together, held slightly apart by rubber-band spacers, and placed in a bag filled with an ERF. The viscosity of the ERF varied with the voltage applied to the tapes, such that it was possible to hold the tapes in the wound condition or slow the speed with which they sprung from the wound to the straight condition. The report describes several potential variations on the basic concept of an ERF-controlled structural member, including compartmentalization of the interior volume to prevent total loss of the ERF in case of a leak and the use of multiple, individually addressable electrode pairs to enable more localized control.

This work was done by Yoseph Bar-Cohen, Zensheu Chang, Moktar Salama, Xiaoqi Bao, and Stewart Sherrit of Caltech; Christopher Jenkins of SDSM&T; and Aleksandra Vinogradov of Montana State University for **NASA's Jet Propulsion Laboratory**. *To obtain a copy of the report, "Controlled gossamer structures deployment and stability using ERF," see TSP's [page 1].*
NPO-30587

Machinery

Hardware, Techniques, and Processes

High-Temperature Switched-Reluctance Electric Motor

Motors like this one would be incorporated into gas turbines as starter/generators.

John H. Glenn Research Center, Cleveland, Ohio

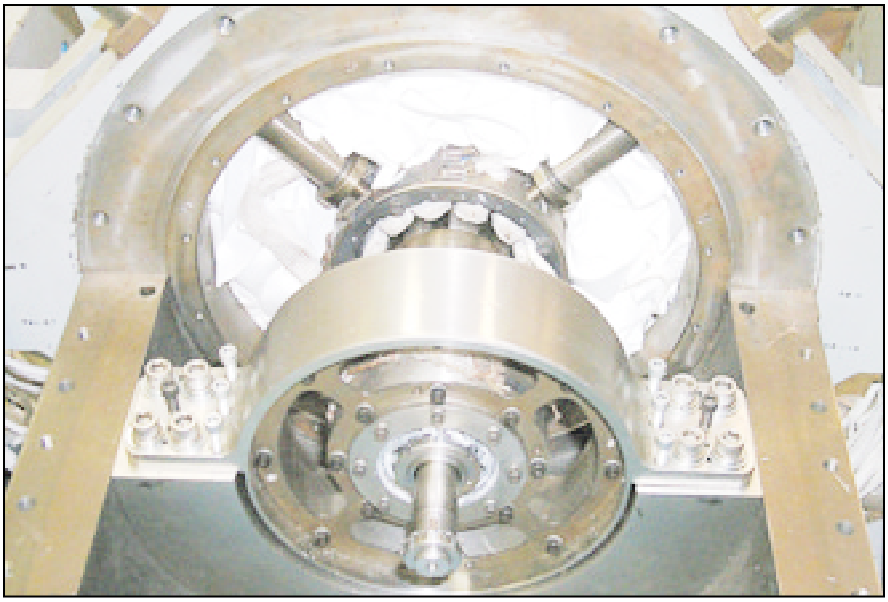

The **High-Temperature Switched-Reluctance Electric Motor**, capable of operating at a speed of 8,000 rpm at a temperature of 1,000 °F (≈540 °C), is a modified version of a magnetic bearing capable of operating at 15,000 rpm at 1,000 °F (≈540 °C).

An eight-pole radial magnetic bearing has been modified into a switched-reluctance electric motor capable of operating at a speed as high as 8,000 rpm at a temperature as high as 1,000 °F (≈540 °C). The motor (see figure) is an experimental prototype of starter-motor/generator units that have been proposed to be incorporated into advanced gas turbine engines and that could operate without need for lubrication or active cooling.

The unique features of this motor are its electromagnet coils and, to some extent, its control software. Heretofore, there has been no commercial-off-the-shelf wire capable of satisfying all of the requirements for fabrication of electromagnet coils capable of operation at temperatures up to 1,000 °F (≈540 °C). The issues addressed in the development of these electromagnet coils included thermal expansion, oxidation, pliability to small bend radii, micro-fretting, dielectric breakdown, tensile strength, potting compound, thermal conduction, and packing factor.

For a test, the motor was supported, along with a rotor of 18 lb (≈8-kg) mass, 3-in. (≈7.6-cm) diameter, 21-in. (≈53-cm) length, on bearings packed with high-temperature grease. The motor was located at the mid span of the rotor and wrapped with heaters. The motor stator was instrumented with thermocouples. At the time of reporting the information for this article, the motor had undergone 14 thermal cycles between room temperature and 1,000 °F (≈540 °C) and had accumulated operating time >27.5 hours at 1,000 °F (≈540 °C).

The motor-controller hardware includes a personal computer equipped with analog-to-digital input and digital-to-analog output cards. The controller software is a C-language code that implements a switched-reluctance motor-control principle: that is, it causes the coils to be energized in a sequence timed to generate a rotating magnetic flux that creates a torque on a scalloped rotor. The controller can operate in an open- or closed-loop mode. In addition, the software has been modified to enable the simultaneous operation of the prototype motor or another, similar apparatus as both a motor and a magnetic bearing. Combined bearing/motor operation has been demonstrated at room temperature but had not yet been demonstrated at high temperature at the time of reporting the information for this article.

This work was done by Gerald Montague, Gerald Brown, Carlos Morrison, Andy Provenza, and Albert Kascak of **Glenn Research Center** *and Alan Palazzolo of Texas A&M University. Further information is contained in a TSP [see page 1].*

Inquiries concerning rights for the commercial use of this invention should be addressed to NASA Glenn Research Center, Commercial Technology Office, Attn: Steve Fedor, Mail Stop 4–8, 21000 Brookpark Road, Cleveland, Ohio 44135. Refer to LEW-17287.

System for Centering a Turbofan in a Nacelle During Tests

The system helps to maintain safety and accuracy.

John H. Glenn Research Center, Cleveland, Ohio

A feedback position-control system has been developed for maintaining the concentricity of a turbofan with respect to a nacelle during acoustic and flow tests in a wind tunnel. The system is needed for the following reasons:

- Thermal and thrust loads can displace the fan relative to the nacelle;
- In the particular test apparatus (see Figure 1), denoted as a rotor-only nacelle (RAN), the struts, vanes, and other stator components of a turbofan engine that ordinarily maintain the required concentricity in the face of thermal and thrust loads are not present; and
- The struts and stator components are not present because it is necessary to provide a flow path that is acoustically "clean" in the sense that the measured noise can be attributed to the fan alone.

The system is depicted schematically in Figure 2. The nacelle is supported by two struts attached to a two-axis traverse table located outside the wind-tunnel wall. Two servomotors acting through 100:1 gearboxes drive the table along the Y and Z axes, which are perpendicular to the axis of rotation. The Y and Z components of the deviation from concentricity are measured by four laser displacement sensors mount-

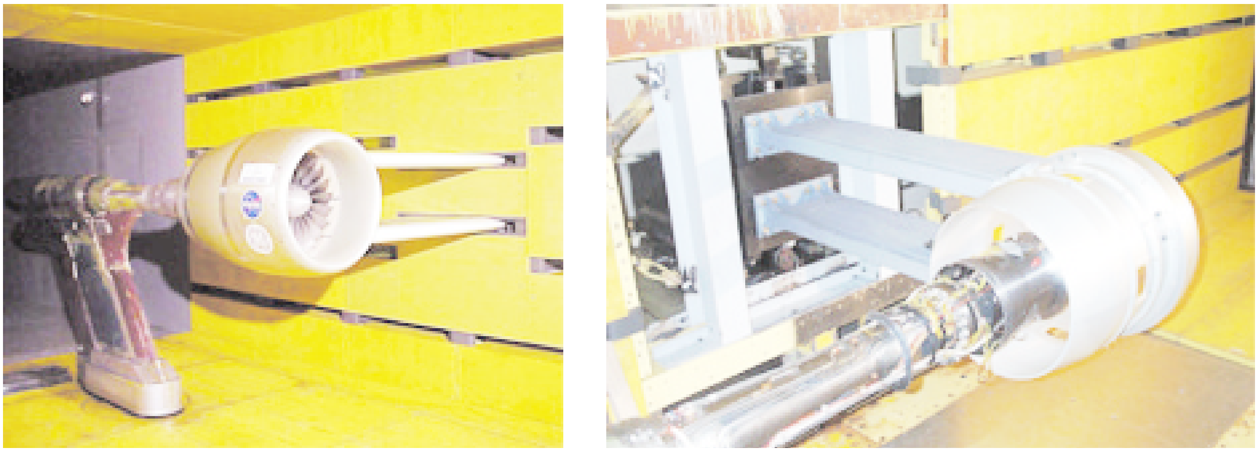

(a) (b)

Figure 1. **RAN System in Test Configuration** is shown in (a), and (b) shows the installation of positioning table behind tunnel wall.

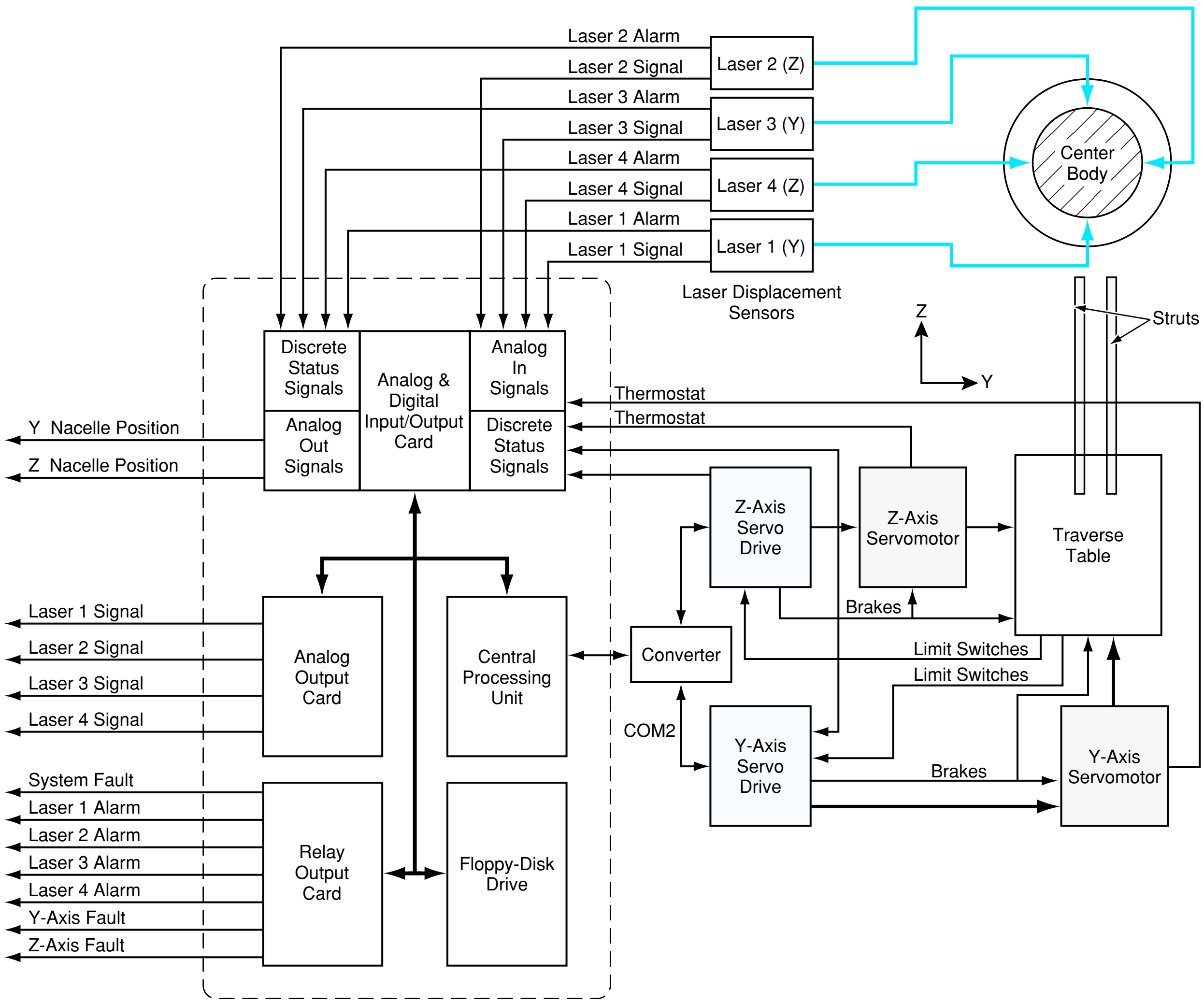

Figure 2. This **Control System** continually adjusts the Z and Y position of the nacelle to minimize eccentricity with respect to the center body.

ed on the nacelle and aimed at reflective targets on the center body, which is part of the fan assembly.

The outputs of the laser displacement sensors are digitized and processed through a personal computer programmed with control software. The control output of the computer commands the servomotors to move the table as needed to restore concentricity. Numerous software and hardware travel limits and alarms are provided to maximize safety. A highly ablative rub strip in the nacelle minimizes the probability of damage in the event that a deviation from concentricity exceeds the radial clearance [<0.004 in. (<0.1 mm)] between the inner surface of the nacelle and the tips of the fan blades.

To be able to prevent an excursion in excess of the tip clearance, the system must be accurate enough to control X and Y displacements to within 0.001 in. (≈0.025 mm). One characteristic essential to such accuracy is sufficient rigidity in the mechanical components of the system to prevent excitation of vibrations in the strut/nacelle subsystem. The need for such a high degree of accuracy prompted a comprehensive analysis of sources of measurement and control errors, followed by rigorous design efforts to minimize these errors. As a result, the design of the system incorporates numerous improvements in hardware, software, and operational procedures.

This work was done by Cameron C. Cunningham, William K. Thompson, Christopher E. Hughes, and Tony D. Shook of **Glenn Research Center**. *Further information is contained in a TSP [see page 1].*

Inquiries concerning rights for the commercial use of this invention should be addressed to NASA Glenn Research Center, Commercial Technology Office, Attn: Steve Fedor, Mail Stop 4–8, 21000 Brookpark Road, Cleveland, Ohio 44135. Refer to LEW-17185.

Hopping Robot With Wheels

Hopping and wheeled motions complement each other.

NASA's Jet Propulsion Laboratory, Pasadena, California

A small prototype mobile robot is capable of (1) hopping to move rapidly or avoid obstacles and then (2) moving relatively slowly and precisely on the ground by use of wheels in the manner of previously reported exploratory robots of the "rover" type. This robot is a descendant of a more primitive hopping robot described in "Minimally Actuated Hopping Robot" (NPO-20911), *NASA Tech Briefs*, Vol. 26, No. 11 (November 2002), page 50. There are many potential applications for robots with hopping and wheeled-locomotion (roving) capabilities in diverse fields of endeavor, including agriculture, search-and-rescue operations, general military operations, removal or safe detonation of land mines, inspection, law enforcement, and scientific exploration on Earth and remote planets.

The combination of hopping and roving enables this robot to move rapidly over very rugged terrain, to overcome obstacles several times its height, and then to position itself precisely next to a desired target. Before a long hop, the robot aims itself in the desired hopping azimuth and at a desired takeoff angle above horizontal. The robot approaches the target through a series of hops and short driving operations utilizing the steering wheels for precise positioning.

Features of this robot include the following:

- An adaptive controlled nonlinear spring mechanism capable of delivering force of specified intensity for hopping;
- Three deployable wheels. Two in front are independently controlled for driving and steering. The third is passive and is located in the rear of the vehicle;
- An autonomous mechanism for self-righting after landing from a hop (described in more detail below);
- A digital camera for acquiring image data;
- Electronic hardware for processing acquired data, computing hopping and roving trajectories, and either wired or wireless communication with a host computer;
- Software for use in sensor-based navigation, trajectory computations, and adjustment of hopping parameters.

The robot has a mass of about 1.5 kg and a minimum volume of about 30 cm^3. It can jump about 1 m high and 2 m horizontally. After landing, the robot rights itself by a combination of actuation of side panels and shifting of its center of mass. The side panels also afford protection at landing and, in future versions, will carry photovoltaic panels for charging batteries.

Once in its upright position, the robot can sit still, move by use of its wheels, or prepare for another hop. The hopping distance can be adjusted by choosing an appropriate takeoff angle and controlling the spring loading. In the present version, images from the onboard camera are sent to a remote operator, who controls the operation of the robot; in future versions, the onboard software will enable autonomous navigation by the robot.

This work was done by Edward Barlow, Nevellie Marzwell, Sawyer Fuller, Paolo Fiorini, Andy Tretton, Joel Burdick, and Steve Schell of Caltech for **NASA's Jet Propulsion Laboratory**. *Further information is contained in a TSP [see page 1].*
NPO-21249

Fabrication Technology

Hardware, Techniques, and Processes

Fabricating Composite-Material Structures Containing SMA Ribbons

Repeatable, predictable structures can be fabricated.

Langley Research Center, Hampton, Virginia

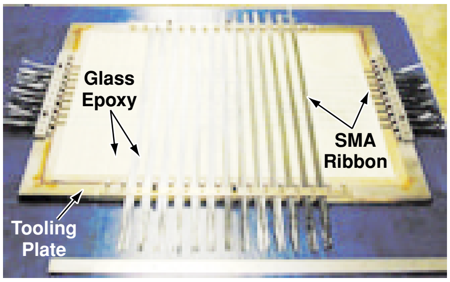

Intermediate Stage of SMAHC Panel Lamination

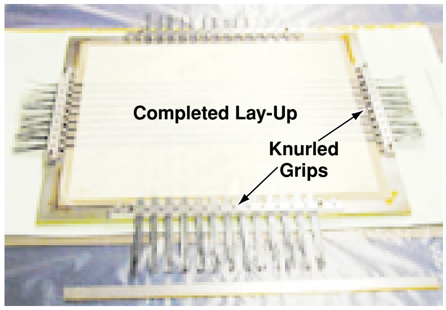

Completed Layup With SMA Ribbon Ends Secured

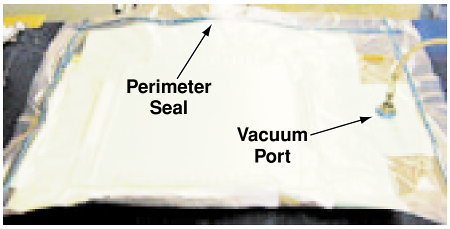

Vacuum-Bagged Laminate Assembly

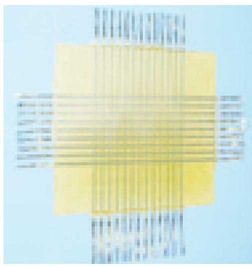
Consolidated SMAHC Laminated Panel

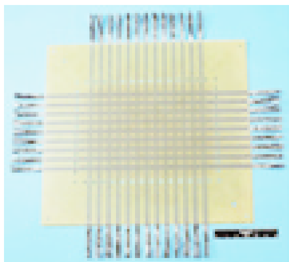
SMAHC Panel Specimen After Final Machining

SMA Ribbons Were Incorporated into an epoxy/fiberglass laminate panel. The panel was then machined to obtain SMAHC beam specimens for testing.

An improved method of designing and fabricating laminated composite-material (matrix/fiber) structures containing embedded shape-memory-alloy (SMA) actuators has been devised. Structures made by this method have repeatable, predictable properties, and fabrication processes can readily be automated.

Such structures, denoted as shape-memory-alloy hybrid composite (SMAHC) structures, have been investigated for their potential to satisfy requirements to control the shapes or thermoelastic responses of themselves or of other structures into which they might be incorporated, or to control noise and vibrations. Much of the prior work on SMAHC structures has involved the use SMA wires embedded within matrices or within sleeves through parent structures. The disadvantages of using SMA wires as the embedded actuators include (1) complexity of fabrication procedures because of the relatively large numbers of actuators usually needed; (2) sensitivity to actuator/matrix interface flaws because voids can be of significant size, relative to wires; (3) relatively high rates of breakage of actuators during curing of matrix materials because of sensitivity to stress concentrations at mechanical restraints; and (4) difficulty of achieving desirable overall volume fractions of SMA wires when trying to optimize the integration of the wires by placing them in selected layers only.

In the present method, one uses SMA ribbons instead of SMA wires. This reduces the number of actuators that must be embedded, thereby making it possible to simplify fabrication processes and to exert better control over the locations and volume fractions of actuators.

In a typical application of this method, one seeks to fabricate one or more structure(s), each comprising an epoxy-matrix/fiber laminate containing one or more embedded SMA ribbons. First, SMA ribbon, as received from the manufacturer packaged on a spool, is removed from the spool and treated to remove the packaging strain. Then by use of a tensile testing machine operating in stroke-control mode, the SMA ribbon is stretched to the amount of prestrain required by the design of the structure. To save time, several parallel lengths of ribbon, separated by spacers and held by grips designed specifically for the purpose, can be stretched simultaneously on the machine.

The figure shows several stages of fabrication of a panel-type structure following elongation of the SMA actuators. Fabrication of the SMAHC laminate proceeds by incorporating lengths of the SMA ribbon at the specified locations during the lamination process. Depending on the design of the specific structure, either the SMA ribbons can be laid up between laminae, or else precisely dimensioned portions of the laminae can be removed and SMA ribbons inserted in the resulting voids to incorporate the SMA ribbons within the laminae. Upon completion of the layup, the free ends of the SMA ribbons are constrained within the knurled mechanical grips to maintain the preset elongation during elevated temperature cure. The entire assembly is then vacuum bagged and subjected to autoclave cure. Subsequent to consolidation, the free ends of the SMA ribbons are released from the grips and the SMAHC structure is machined to final dimensions.

This work was done by Travis L. Turner, Roberto J. Cano, and Cynthia L. Lach of **Langley Research Center**. *Further information is contained in a TSP [see page 1].*
LAR-16273

Mathematics and Information Sciences

Hardware, Techniques, and Processes

Optimal Feedback Control of Thermal Networks

A systematic approach to design has been devised.

NASA's Jet Propulsion Laboratory, Pasadena, California

An improved approach to the mathematical modeling of feedback control of thermal networks has been devised. Heretofore software for feedback control of thermal networks has been developed by time-consuming trial-and-error methods that depend on engineers' expertise. In contrast, the present approach is a systematic means of developing algorithms for feedback control that is optimal in the sense that it combines performance with low cost of implementation. An additional advantage of the present approach is that a thermal engineer need not be expert in control theory.

Thermal networks are lumped-parameter approximations used to represent complex thermal systems. Thermal networks are closely related to electrical networks commonly represented by lumped-parameter circuit diagrams. Like such electrical circuits, thermal networks are mathematically modeled by systems of differential-algebraic equations (DAEs) — that is, ordinary differential equations subject to a set of algebraic constraints. In the present approach, emphasis is placed on applications in which thermal networks are subject to constant disturbances and, therefore, integral control action is necessary to obtain steady-state responses.

The mathematical development of the present approach begins with the derivation of optimal integral-control laws via minimization of an appropriate cost functional that involves augmented state vectors. Subsequently, classical variational arguments provide optimality conditions in the form of the Hamiltonian equations for the standard linear-quadratic-regulator (LQR) problem. These equations are reduced to an algebraic Riccati equation (ARE) with respect to the augmented state vector. The solution of the ARE leads to the direct computation of the optimal proportional- and integral-feedback control gains.

In cases of very complex networks, large numbers of state variables make it difficult to implement optimal controllers in the manner described in the preceding paragraph. Therefore, another important element of the present approach is consideration of decentralized control (that is, the use of nominally suboptimal controllers, each affecting only part of the network). Numerical tests of an algorithm that computes feedback gains for decentralized control have shown that the performances of the decentralized controllers are comparable to the performances of the corresponding optimal controllers (see figure). In particular, it was observed that decentralized controllers might require a little more energy than their optimal counterparts; however, this is a small price to pay for the simplification of controller structures that can be achieved. Further, the lower cost of implementation of much simpler feedback loops in decentralized control outweighs the extra amount of energy that decentralized controllers might require.

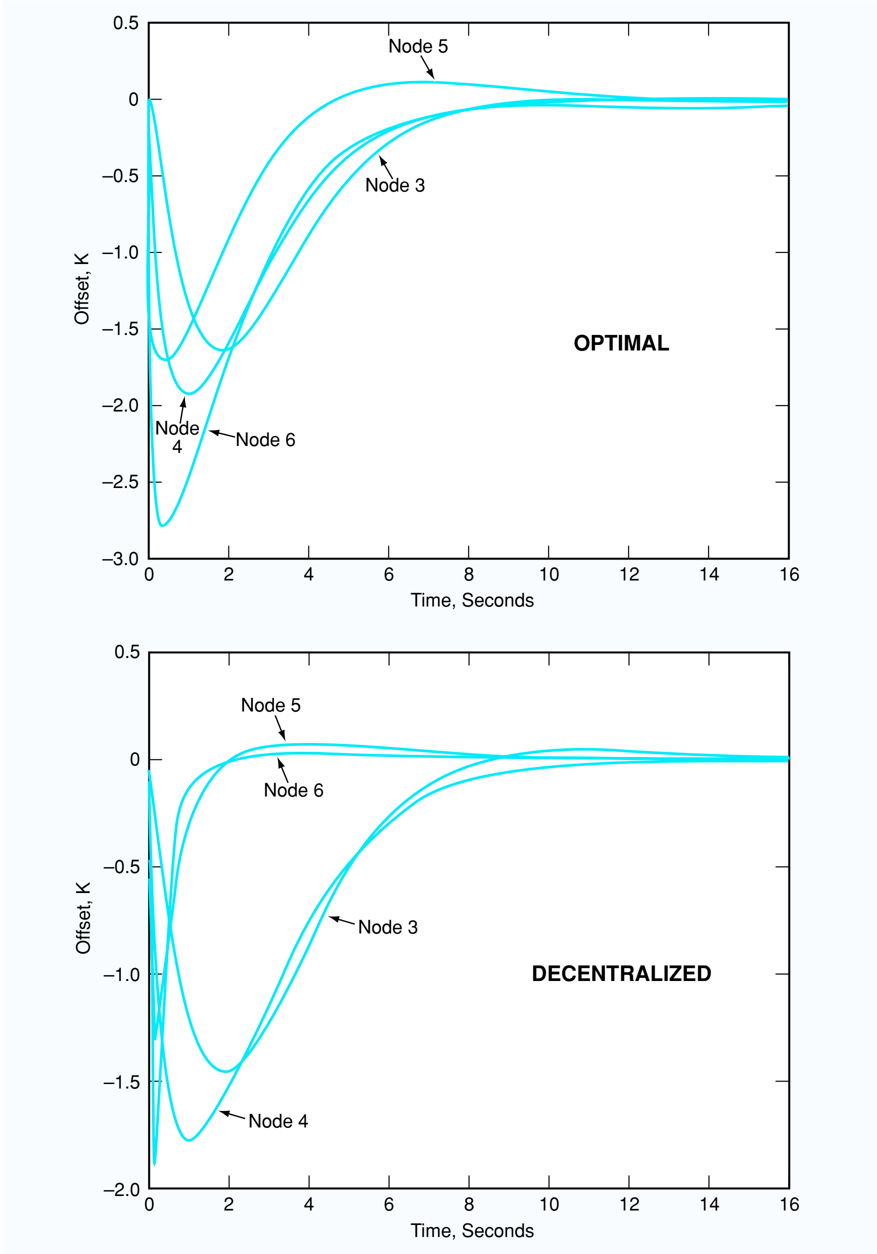

The **Time-Dependent Offsets of Four Nodes** of a 9-node network were computed in a numerical test of optimal- and decentralized-control laws. Both control laws yield smooth temperature histories, without oscillations or large overshoots, and both require about the same amount of time to achieve nearly zero offset (where offset as used here signifies the difference between the actual and desired temperatures of a given node).

This work was done by Miltiadis Papalexandris of Caltech for **NASA's Jet Propulsion Laboratory**. *Further information is contained in a TSP [see page 1].*

This software is available for commercial licensing. Please contact Don Hart of the California Institute of Technology at (818) 393-3425. Refer to NPO-30354.

Artifacts for Calibration of Submicron Width Measurements

Dimensional tolerances as small as 1 nm should be possible.

NASA's Jet Propulsion Laboratory, Pasadena, California

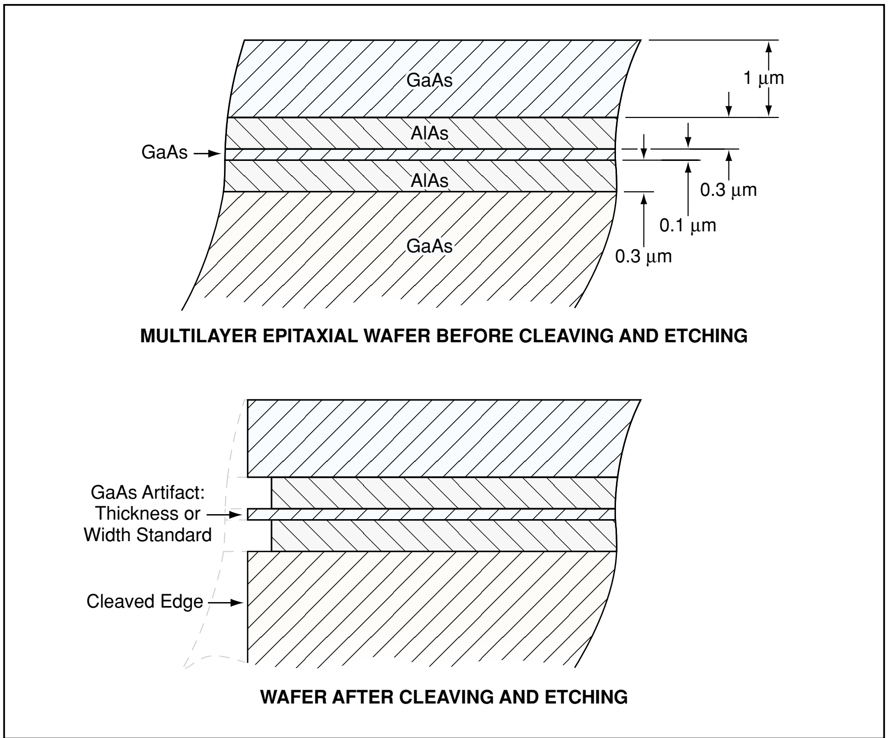

An **Artifact With a Reproducible Thickness of 0.1 µm** is made by MBE of GaAs and AlAs followed by differential etching. The basic concept is not limited to the GaAs/AlAs material system: other semiconductor material systems amenable to MBE and differential etching could be used.

Artifacts that are fabricated with the help of molecular-beam epitaxy (MBE) are undergoing development for use as dimensional calibration standards with submicron widths. Such standards are needed for calibrating instruments (principally, scanning electron microscopes and scanning probe microscopes) for measuring the widths of features in advanced integrated circuits. Dimensional calibration standards fabricated by an older process that involves lithography and etching of trenches in (110) surfaces of single-crystal silicon are generally reproducible to within dimensional tolerances of about 15 nm. It is anticipated that when the artifacts of the present type are fully developed, their critical dimensions will be reproducible to within 1 nm. These artifacts are expected to find increasing use in the semiconductor-device and integrated-circuit industries as the width tolerances on semiconductor devices shrink to a few nanometers during the next few years.

Unlike in the older process, one does not rely on lithography and etching to define the critical dimensions. Instead, one relies on the inherent smoothness and flatness of MBE layers deposited under controlled conditions and defines the critical dimensions as the thicknesses of such layers. An artifact of the present type is fabricated in two stages (see figure): In the first stage, a multilayer epitaxial wafer is grown on a very flat substrate. In the second stage, the wafer is cleaved to expose the layers, then the exposed layers are differentially etched (taking advantage of large differences between the etch rates of the different epitaxial layer materials).

The resulting structure includes narrow and well-defined trenches and a shelf with thicknesses determined by the thicknesses of the epitaxial layers from which they were etched. Eventually, it should be possible to add a third fabrication stage in which durable, electronically inert artifacts could be replicated in diamondlike carbon from a master made by MBE and etching as described above.

This work was done by Frank Grunthaner and Paula Grunthaner of Caltech and Charles Bryson III of Surface/Interface, Inc., for **NASA's Jet Propulsion Laboratory**. *Further information is contained in a TSP [see page 1].*

In accordance with Public Law 96-517, the contractor has elected to retain title to this invention. Inquiries concerning rights for its commercial use should be addressed to

Intellectual Property group
JPL
Mail Stop 202-233
4800 Oak Grove Drive
Pasadena, CA 91109
(818) 354-2240

Refer to NPO-21130, volume and number of this NASA Tech Briefs *issue, and the page number.*

Navigating a Mobile Robot Across Terrain Using Fuzzy Logic

This strategy is modeled on the actions of a human driver.

NASA's Jet Propulsion Laboratory, Pasadena, California

A strategy for autonomous navigation of a robotic vehicle across hazardous terrain involves the use of a measure of traversability of terrain within a fuzzy-logic conceptual framework. This navigation strategy requires no *a priori* information about the environment. Fuzzy logic was selected as a basic element of this strategy because it provides a formal methodology for representing and implementing a human driver's heuristic knowledge and operational experience.

Within a fuzzy-logic framework, the attributes of human reasoning and decision-making can be formulated by simple IF (antecedent), THEN (consequent) rules coupled with easily understandable and natural linguistic representations. The linguistic values in the rule antecedents convey the imprecision associated with measurements taken by sensors onboard a mobile robot, while the linguistic values in the rule consequents represent the vagueness inherent in the reasoning processes to generate the control actions. The operational strategies of the human expert driver can be transferred, via fuzzy logic, to a robot-navigation strategy in the form of a set of simple conditional statements composed of linguistic variables. These linguistic variables are defined by fuzzy sets in accordance with user-defined membership functions. The main advantages of a fuzzy navigation strategy lie in the ability to extract heuristic rules from human experience and to obviate the need for an analytical model of the robot navigation process.

The basic building block of the present navigation strategy is a behavior, defined here as a representation of a specific sequence of actions aimed at attaining a given desired objective. Each behavior comprises a set of fuzzy-logic rules of the form

IF C, THEN A,

where the condition C is composed of fuzzy input variables and fuzzy connectives (AND, OR, NOT), and the action A is a fuzzy output variable. Such an IF, THEN rule represents a typical rule in a set of natural linguistic rules that express the actions taken by an expert human driver based on the prevalent conditions. The output of each behavior describable by such a rule set is a recommendation over all possible control actions from the perspective of attaining the objective.

Multiple behaviors, each aimed at one specific goal, can be active simultaneously in the navigation strategy. Blending of multiple behaviors is implemented by combining the outputs (recommendations) of all the behaviors using gain rules of the form

IF S, THEN K,

where S is a logical statement that describes a physical situation, and K represents a fuzzy expression of the gains with which the recommendation of the individual behaviors are weighted in the prevalent situation. The result of the weighted combination of recommendations is then issued as a command to the wheel actuators of the mobile robot.

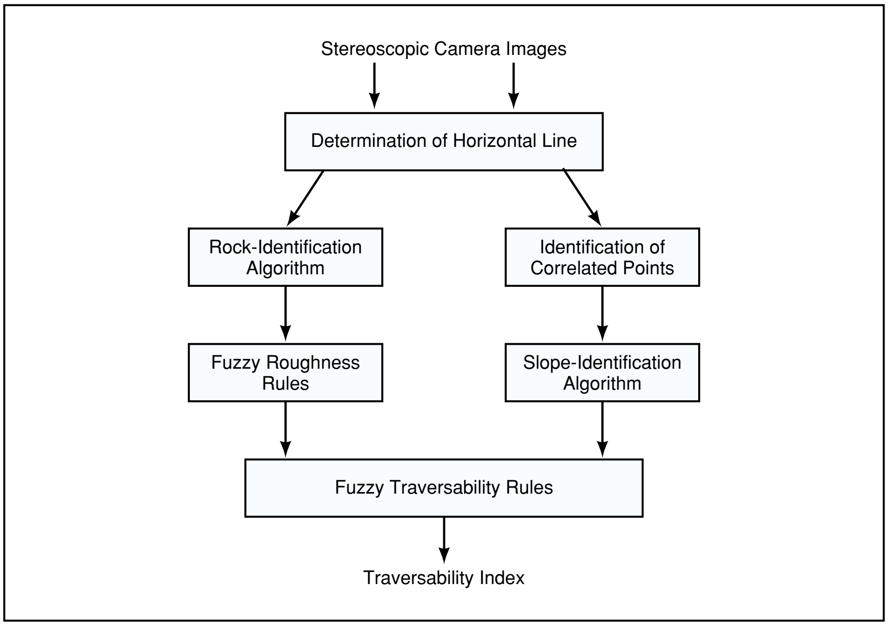

Image Data Acquired by Onboard Stereoscopic Cameras is processed into terrain-quality information and summarized in a fuzzy traversability index.

The present robot-navigation strategy involves three such behaviors, denoted seek-goal, traverse-terrain, and avoid-obstacle:

- The navigation rules for the seek-goal behavior utilize the global information about the goal position to generate the steering and speed commands that drive the robot to the designated destination.
- The navigation rules for the traverse-terrain behavior utilize regional information about the quality of the terrain to produce steering and speed commands that guide the robot toward the safest and the most traversable terrain. The regional terrain-quality information is generated from readings of onboard sensors by use of a set of fuzzy-logic rules. This behavior constitutes a major novel aspect of the present strategy (see figure).
- The navigation rules for the avoid-obstacle behavior employ local information about obstacles en route to develop steering and speed commands to maneuver the robot around the obstacles.

The recommendations of these three behaviors are blended through gains or weighting factors to generate the final steering and speed commands to be executed by the wheel actuators of the robot. The gains are also generated by fuzzy-logic rules that take into account the current status of the robot.

This work was done by Homayoun Seraji, Ayanna Howard, and Bruce Bon of Caltech for **NASA's Jet Propulsion Laboratory**. *Further information is contained in a TSP [see page 1].*

This software is available for commercial licensing. Please contact Don Hart of the California Institute of Technology at (818) 393-3425. Refer to NPO-21199.

Designing Facilities for Collaborative Operations

A methodology is emerging from efforts to design a mission operations facility.

NASA's Jet Propulsion Laboratory, Pasadena, California

A methodology for designing operational facilities for collaboration by multiple experts has begun to take shape as an outgrowth of a project to design such facilities for scientific operations of the planned 2003 Mars Exploration Rover (MER) mission. The methodology could also be applicable to the design of military "situation rooms" and other facilities for terrestrial missions.

It was recognized in this project that modern mission operations depend heavily upon the collaborative use of computers. It was further recognized that tests have shown that layout of a facility exerts a dramatic effect on the efficiency and endurance of the operations staff. The facility designs (for example, see figure) and the methodology developed during the project reflect this recognition.

One element of the methodology is a metric, called effective capacity, that was created for use in evaluating proposed MER operational facilities and may also be useful for evaluating other collaboration spaces, including meeting rooms and military situation rooms. The effective capacity of a facili-

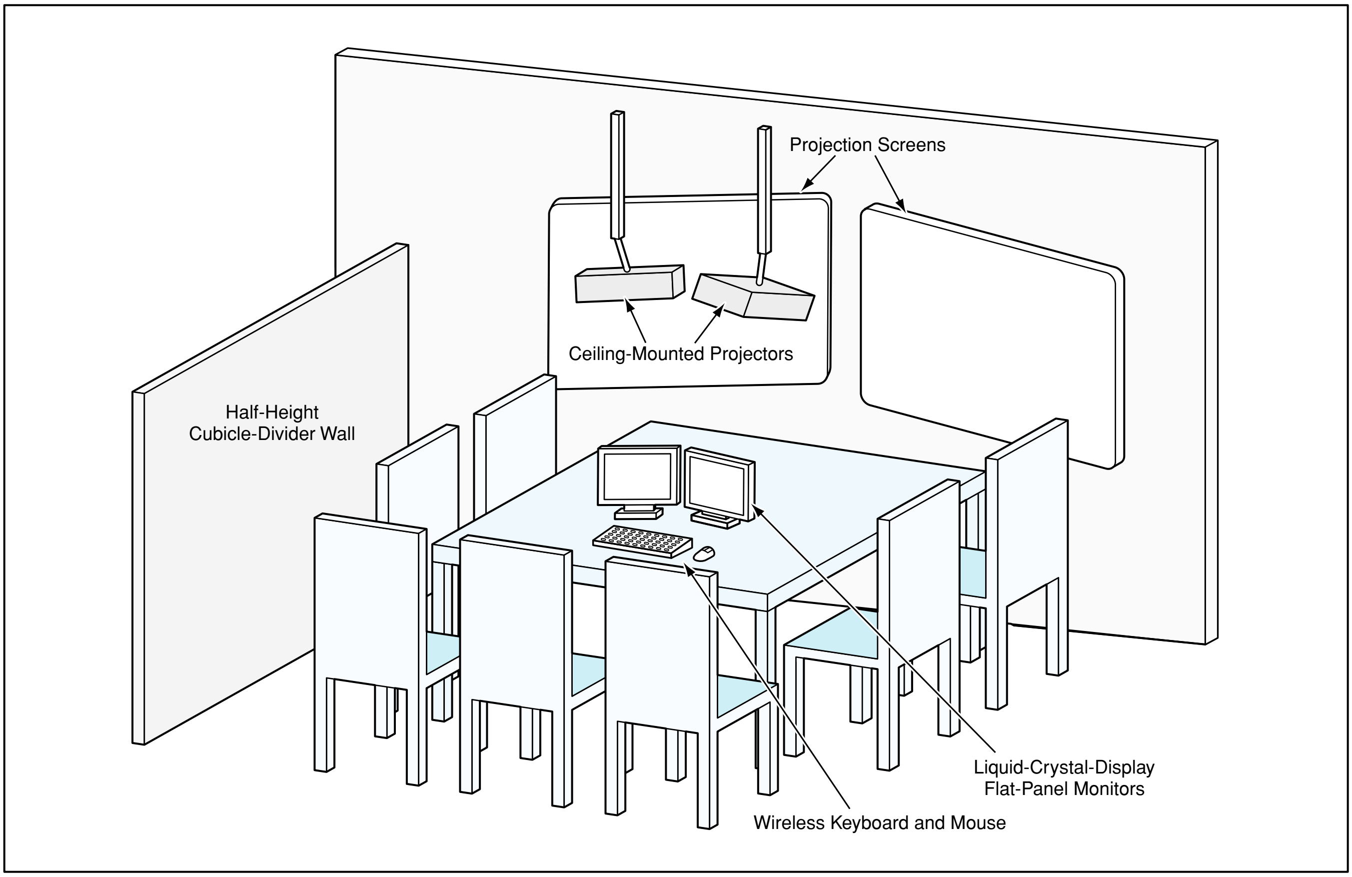

This **Proposed Work-Space Design** would enable seven participants to collaborate while using a single workstation.

ty is defined as the number of people in the facility who can be meaningfully engaged in its operations. A person is considered to be meaningfully engaged if the person can (1) see, hear, and communicate with everyone else present; (2) see the material under discussion (typically data on a piece of paper, computer monitor, or projection screen); and (3) provide input to the product under development by the group. The effective capacity of a facility is less than the number of people that can physically fit in the facility. For example, a typical office that contains a desktop computer has an effective capacity of ≈4, while a small conference room that contains a projection screen has an effective capacity of around 10. Little or no benefit would be derived from allowing the number of persons in an operational facility to exceed its effective capacity: At best, the operations staff would be underutilized; at worst, operational performance would deteriorate.

Elements of this methodology were applied to the design of three operations facilities for a series of rover field tests. These tests were observed by human-factors researchers and their conclusions are being used to refine and extend the methodology to be used in the final design of the MER operations facility.

Further work is underway to evaluate the use of personal digital assistant (PDA) units as portable input interfaces and communication devices in future mission operations facilities. A PDA equipped for wireless communication and Ethernet, Bluetooth, or another networking technology would cost less than a complete computer system, and would enable a collaborator to communicate electronically with computers and with other collaborators while moving freely within the virtual environment created by a shared immersive graphical display.

This work was done by Jeffrey Norris, Mark Powell, Paul Backes, Robert Steinke, and Kam Tso of Caltech and Roxana Wales of Ames Research Center for **NASA's Jet Propulsion Laboratory**. *Further information is contained in a TSP [see page 1].*
NPO-30457

Life Sciences

Hardware, Techniques, and Processes

Quantitating Iron in Serum Ferritin by Use of ICP-MS

Ferritin associated with inflammation can be distinguished from ferritin associated with hemochromatosis.

Lyndon B. Johnson Space Center, Houston, Texas

A laboratory method has been devised to enable measurement of the concentration of iron bound in ferritin from small samples of blood (serum). Derived partly from a prior method that depends on large samples of blood, this method involves the use of an inductively-coupled-plasma mass spectrometer (ICP-MS).

Ferritin is a complex of iron with the protein apoferritin. Heretofore, measurements of the concentration of serum ferritin (as distinguished from direct measurements of the concentration of iron in serum ferritin) have been used to assess iron stores in humans. Low levels of serum ferritin could indicate the first stage of iron depletion. High levels of serum ferritin could indicate high levels of iron (for example, in connection with hereditary hemochromatosis — an iron-overload illness that is characterized by progressive organ damage and can be fatal). However, the picture is complicated: A high level of serum ferritin could also indicate stress and/or inflammation instead of (or in addition to) iron overload, and low serum iron concentration could indicate inflammation rather than iron deficiency. Only when concentrations of both serum iron and serum ferritin increase and decrease together can the patient's iron status be assessed accurately. Hence, in enabling accurate measurement of the iron content of serum ferritin, the present method can improve the diagnosis of the patient's iron status.

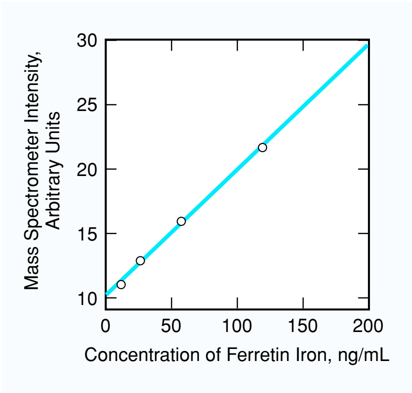

The **Response of the ICP-MS** is a linear function of the concentration of ferritin iron.

The prior method of measuring the concentration of iron involves the use of an atomic-absorption spectrophotometer with a graphite furnace. The present method incorporates a modified version of the sample-preparation process of the prior method. First, ferritin is isolated; more specifically, it is immobilized by immunoprecipitation with rabbit antihuman polyclonal antibody bound to agarose beads. The ferritin is then separated from other iron-containing proteins and free iron by a series of centrifugation and wash steps. Next, the ferritin is digested with nitric acid to extract its iron content. Finally, a micronebulizer is used to inject the sample of the product of the digestion into the ICP-MS for analysis of its iron content. The sensitivity of the ICP-MS is high enough to enable it to characterize samples smaller than those required in the prior method (samples can be 0.15 to 0.60 mL).

The method has been validated in experiments. In one set of experiments, the linearity of the ICP-MS response (see figure) was established by use of a high-concentration sample diluted to several known lower concentrations. In another set of experiments involving spiked recovery (in which known amounts of iron were added to samples from which natural iron had been stripped), the fraction of added iron recovered was found to lie in the range of 0.96 ± 0.10. In still other experiments, the inter- and intra-assay coefficients of variation for three control samples were found to be 0.12 and 0.09, respectively. These findings suggest that the method can be used to distinguish elevated ferritin due to inflammation and that due to iron overload, using small samples of serum containing ferritin iron at concentrations as low as 10 ng/mL.

This work was done by Scott M. Smith of **Johnson Space Center** *and Patricia L. Gillman of Enterprise Advisory Service, Inc. Further information is contained in a TSP* *[see page 1].*
MSC-23130

National Aeronautics and
Space Administration